JOURNAL OF PETROLOGY | VOLUME 45 | NUMBER 2 | PAGES 343–367 | 2004 | DOI: 10.1093/petrology/egg090

Chemical Variations in Peridotite Xenoliths from Vitim, Siberia: Inferences for REE and Hf Behaviour in the Garnet-Facies Upper Mantle

DMITRI IONOV*

LABORATOIRE DE TECTONOPHYSIQUE (UMR 5568 CNRS), ISTEEM, UNIVERSITÉ MONTPELLIER 2, 34095 MONTPELLIER, FRANCE

LGCA, MAISON DES GÉOSCIENCES, UNIVERSITÉ DE GRENOBLE, 38041 GRENOBLE, FRANCE

RECEIVED NOVEMBER 18, 2002; ACCEPTED JULY 18, 2003

Peridotite xenoliths in a Miocene picrite tuff from the Vitim volcanic province east of Lake Baikal, Siberia, are samples of the off-craton lithospheric mantle that span a depth range from the spinel to garnet facies in a mainly fertile domain. Their major and trace element compositions show some scatter (unrelated to sampling or analytical problems), which is not consistent with different degrees of partial melting or metasomatism. Some spinel peridotites and, to a lesser degree, garnet-bearing peridotites are depleted in heavy rare earth elements (HREE) relative to middle REE (MREE), whereas some garnet peridotites are enriched in HREE relative to MREE, with Lu abundances much higher than in primitive mantle estimates. Clinopyroxenes from several spinel peridotites have HREE-depleted patterns, which are normally seen only in clinopyroxenes coexisting with garnet. Garnets in peridotites with similar modal and major element compositions have a broad range of Lu and Yb abundances. Overall, HREE are decoupled from MREE and Hf and are poorly correlated with partial melting indices. It appears that elements with high affinity to garnet were partially redistributed in the Vitim peridotite series following partial melting, with few effects for other elements. The Lu–Hf decoupling may disturb Hf-isotope depletion ages and their correlations with melting indices.

KEY WORDS: *garnet peridotite; lithospheric mantle; Lu–Hf isotope system; Siberia; trace elements*

INTRODUCTION

Garnet lherzolite is the most common rock type in the upper mantle. Experimental evidence and studies of mantle samples indicate that the lithospheric mantle below a depth of about 60 km is largely made up of garnet-bearing peridotites (e.g. Caroll-Webb & Wood, 1986; Brey & Köhler, 1990; Menzies, 1990; Ionov *et al.*, 1993; Kempton *et al.*, 1999*b*; Stern *et al.*, 1999). Garnet appears to be stable also in the source regions of many mantle-derived volcanic rocks (Halliday, 1999; Presnall *et al.*, 2002). Much of our knowledge of the chemical composition of the upper mantle comes from studies of peridotite massifs and xenoliths in basalts. However, those direct mantle samples commonly belong to the low-pressure spinel lherzolite facies and represent only the uppermost lithospheric mantle. Garnet peridotite xenoliths in kimberlites are typically not representative of the mantle beyond cratons (Boyd, 1989; Ionov *et al.*, 1993). As a result, comprehensive geochemical information on the off-craton garnet-facies mantle remains scarce, in particular compared with the large amount of data obtained recently on spinel peridotites. Further studies of garnet-bearing peridotite xenoliths in basalts are necessary to address the poor geochemical knowledge of the largest upper-mantle reservoir.

Peridotite xenoliths in Miocene picritic tuffs from the Vitim plateau in Siberia (Ashchepkov *et al.*, 1989) are arguably some of the best currently available samples

*Present address: Max-Planck-Institut für Chemie, Abteilung Geochemie, Postfach 3060, D-55020 Mainz, Germany. Telephone: +49-6131-305361. Fax: +49-6131-371051.
E-mail: ionov@mpch-mainz.mpg.de

of garnet-facies off-craton mantle. Unlike most other off-craton xenolith suites worldwide, the majority of the peridotite xenoliths in this locality (some 80%) are garnet and garnet–spinel lherzolites. Many of these xenoliths are large (≥10–20 cm) and relatively fresh (compared with highly altered xenoliths in kimberlites) and therefore they may be representative of the garnet-bearing mantle in this region.

Ionov *et al.* (1993) described the petrography, and bulk-rock and mineral major element compositions for a large set of garnet and spinel peridotite xenoliths from the Vitim picritic tuffs. They also outlined the distribution of rare earth elements (REE) and some other minor and trace elements in both whole rocks and pure mineral separates based on instrumental neutron activation analysis (INAA). Ionov & Hofmann (1995) reported analyses by inductively coupled plasma mass spectrometry (ICP-MS) of vein amphibole separated from Vitim xenoliths. Glaser *et al.* (1999) provided laser-ablation (LA)–ICP-MS analyses for four garnet peridotite and two spinel peridotite xenoliths. Litasov *et al.* (2000) examined the major and trace element composition of minerals in pyroxenite xenoliths from Vitim.

A major objective of this study is to characterize the trace element composition of the major rock types in the mantle beneath Vitim: garnet, spinel and garnet–spinel peridotites, based on solution ICP-MS analyses of whole-rock samples and LA–ICP-MS and ion-microprobe analyses of minerals (mostly clinopyroxene and garnet). The residence and inter-mineral element distribution in garnet peridotites, in particular, is relevant to the interpretation of Lu–Hf and Sm–Nd isotope data, because garnet strongly fractionates REE. These results, together with major element compositions, are examined to outline large-scale chemical variations in the lithospheric mantle section (from spinel to garnet facies) beneath Vitim, as well as to explore local chemical heterogeneities in the garnet-facies mantle. It is demonstrated that heavy REE (HREE) abundances and HREE/middle REE (MREE) values in many whole-rock Vitim peridotites and their minerals cannot be produced by different degrees of partial melting of a fertile source, but may be consistent with some local HREE redistribution after partial melting. These local chemical heterogeneities, possibly related to the transition from spinel to garnet peridotite facies in melting residues, may have important consequences for the interpretation of Lu–Hf isotope data for garnet peridotites.

GEOLOGICAL SETTING AND SAMPLES

The Vitim plateau is located some 200–250 km east of central Lake Baikal, in the region broadly referred to in Russian as Transbaikalie (Fig. 1). Cenozoic basaltic lava flows cover an area about 100 km across in the central part of the plateau (elevations of 1000–1200 m), which also contains the eroded remains of several eruption centres. The Vitim basaltic field, together with several other areas of basaltic volcanism south of the Siberian platform, has been commonly considered as part of the Baikal rift zone. Furthermore, several recent xenolith studies (Glaser *et al.*, 1999; Litasov *et al.*, 2000) assumed, following Zorin (1981), that the rift zone is underlain by a large-scale 'asthenospheric bulge', which recently eroded much of the lithospheric mantle. By contrast, recent tectonic and geophysical studies (e.g. Petit *et al.*, 1998), together with reassessment of the earlier data, have found no evidence for large-scale lithospheric thinning in the central and northern Baikal rift zone nearest the Vitim plateau [see review by Ionov (2002)]. Because the Vitim plateau is clearly distinct from the Baikal rift proper in terms of its relief and tectonic setting, it may be more appropriate to consider the Vitim volcanic field as part of the broad diffuse area of Cenozoic basaltic volcanism between the Siberian and North China cratons.

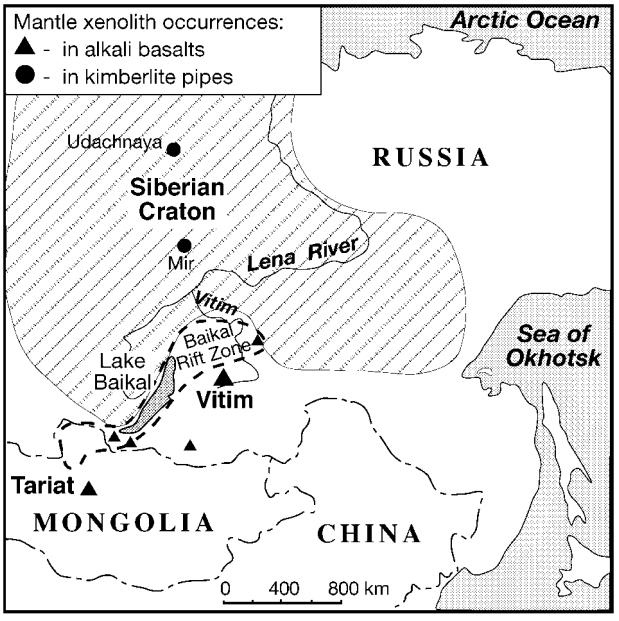

Fig. 1. A sketch map showing the location of the Vitim volcanic field and some other mantle xenolith occurrences in central and northern Asia. It should be noted that the Vitim field is located outside the Baikal rift zone (dashed contour) [Ionov (2002) and references therein].

The xenoliths for this study come from a picrite tuff deposit in the eastern part of the Vitim plateau [see Ionov *et al.* (1993) for a detailed locality map]. The tuffs have been excavated for road construction, and most xenoliths for this and many other studies have been collected on the side of the road near the tuff pit.

The same locality was referred to as 'Bereya area' and 'picrobasalt quarry' by Glaser *et al.* (1999) and Litasov *et al.* (2000). Precise dating of the picrite tuff is problematic because of alteration and the presence of abundant xenolithic material. K–Ar analyses of handpicked material have yielded Middle Miocene age estimates between 15 ± 2 and 18 ± 1 Ma (I. Ashchepkov, personal communication, 2000), whereas Esin *et al.* (1995) obtained an K–Ar age of 16·3 ± 1·1 Ma. Most other volcanic rocks in the area are much younger (≤8 Ma); some host spinel and garnet–spinel xenoliths. The Miocene age of the host rocks further indicates that the mantle beneath Vitim is not likely to have been directly affected, at the time of xenolith entrapment in the picritic magma, by the development of the Baikal rift, which was most active in the last 3–4 Myr.

About half the samples in this study (Table 1) are xenoliths previously described by Ionov *et al.* (1993). Some of those xenoliths (e.g. 313-1 to 313-37) might have been too small (6–10 cm) to yield representative whole-rock samples of coarse-grained garnet peridotites (Boyd, 1989; Boyd *et al.*, 1997). Additional xenoliths (10–25 cm in longest dimension) were selected for this study to provide whole-rock samples of ≥0·5 kg. The xenoliths were cut using a diamond saw; once the rims had been removed, their interiors were crushed either in a hand steel mortar or in a bench-top jaw crusher, carefully cleaned after each sample to avoid cross-contamination. Aliquots of the crushed samples were ground in an agate mortar to produce whole-rock powders. Pyroxene and garnet grains (0·5–1 mm in size) were handpicked from other aliquots and put on mounts for *in situ* analyses. Fresh-looking cryptocrystalline volcanic material was handpicked from crushed picrite tuff and leached in diluted HCl to remove alteration products that may have been overlooked during handpicking.

ANALYTICAL METHODS

Major elements in bulk rocks were determined by X-ray fluorescence (XRF) wavelength-dispersive spectrometry at Niigata University using low-dilution fused beads [see Takazawa *et al.* (2003) for analytical details]. Before producing the beads, the whole-rock powders were heated to 900°C for ≥6 h; the ignition is believed to oxidize all iron to Fe_2O_3. Major element compositions of minerals were determined in polished thin sections by wavelength-dispersive electron probe microbeam analysis (EPMA) at Macquarie University (Sydney) with a Cameca SX-50 instrument and at Montpellier with a Cameca SX-100 instrument. The microprobes were used with an 15 kV accelerating voltage and sample current of 20 nA. Standards were natural and synthetic minerals; matrix corrections were by the PAP method. Modal abundances were calculated by mass balance of mineral and whole-rock compositions using least-squares regression.

Whole-rock powders (~100 mg) for solution ICP-MS analyses were dissolved in HF–$HClO_4$ mixtures. Dried samples were taken up in HNO_3 and diluted to 1:1000 (in 2% HNO_3) shortly before the analysis. About half the analyses were carried out at Grenoble University on a Fisons (VG-Elemental) PQ2+Turbo (PlasmaQuad II+) instrument. Sample solutions were spiked with Tm; BHVO-1 was used for calibration. Another series of samples was analysed on a similar instrument at Montpellier mainly following the method of Ionov *et al.* (1992). Two sets of composite synthetic standards were used for calibration; samples were spiked with In and Bi for drift correction. Appropriate synthetic solutions were used in Grenoble and Montpellier to correct for oxide interference. Several whole-rock analyses were also carried out at Niigata on an HP4500 instrument following the technique reported by Takazawa *et al.* (2003). Chemical blanks and 2–3 international reference materials were run with each sample batch. Trace element composition of garnet and pyroxenes was determined in polished grain mounts by LA–ICP-MS at Macquarie University on a Perkin–Elmer Sciex ELAN 5100 instrument coupled with a UV (266 nm) laser. The laser was operated with 1 mJ/pulse energy at 4 Hz and produced pits about 50 μm in diameter. NIST 610 glass was used as calibration standard for all samples, with ^{44}Ca as internal standard. Detection limits for most elements ranged from 0·01 to 0·2 ppm. Analytical precision is 2–5% (1σ) at the ppm level (Norman *et al.*, 1996). Most analyses were carried out using He–Ar mixtures as the carrier gas, with improved precision and detection limits. Trace elements were also determined in profiles across garnet and clinopyroxene grains by secondary ion mass spectrometry (SIMS) on a recently upgraded Cameca 4f instrument in Montpellier, following procedures reported by Bottazzi *et al.* (1994).

PETROGRAPHY

The samples analysed in this study are listed in Table 1 together with P–T estimates, modal compositions and information about the type of analytical work performed on each xenolith. Three major rock types are identified in the xenoliths: spinel, garnet–spinel and garnet peridotites (Ionov *et al.*, 1993). Their textures can be broadly defined as protogranular, with minor differences between the rock types. All the xenoliths are medium to coarse grained. Strongly deformed (sheared) rocks are extremely rare in the xenolith suite (Ashchepkov, 1991; Glaser *et al.*, 1999) and are not considered here.

Table 1: List of samples with sources of data and estimates of P, T *and modal compositions*

Sample no.	EPMA	WR XRF	*P* (kbar)		*T*(°C) (Ca-Op)		Modal composition (wt %)					WR ICP-MS	LA–ICP-MS
			core	rim	core	rim	Ol	Op	Cp	Gr	Sp		
Garnet peridotites													
313-1	(1)	(2)	19·4	21·0	953	1007	60·8	13·7	12·1	13·4		(1)	
313-2	(1)	(2)	20·3	20·4	1026	1044	57·8	21·8	13·8	6·6		(1)	
313-3	(1)	(2)	20·8	20·3	983	1008	61·1	12·7	14·3	11·9		(1)	cp, gr
313-6	(2)	(2)	18·1		1023		63·7	12·1	12·9	11·3		(1)	cp, gr, op
313-8	(1)	(2)	20·3	20·3	1004	1049	57·0	13·4	15·6	14·0		(1)	
313-54	(1)	(2)	21·4	21·7	1019	1074	59·4	14·6	13·9	12·1		(3)	cp, gr
313-102	(1)	(1)	22·9	22·1	1053	1143	55·9	15·6	15·8	12·8		(1)	cp, gr
313-104	(1)	(1)	21·1	20·9	1037	1089	56·9	18·7	15·8	8·7		(1)	cp, gr
313-105	(1)	(2)	21·0	20·5	1025	1088	59·1	20·4	11·9	8·7		(3)	cp, gr
313-106	(1)	(1)	20·4	21·1	997	1040	63·3	14·5	13·6	8·6		(1)	cp, gr
313-112	(1)	(1)	23·1	23·1	1041	1054	55·6	21·2	11·1	12·2		(1)	cp, gr
313-240	(1)	(1)	20·7	21·3	1014	1112	64·2	15·3	11·7	8·7		(1)	cp, gr
313-241	(1)	(1)	20·9	21·6	1012	1091	62·5	14·9	12·6	10·1		(1)	cp, gr
Garnet–spinel peridotites													
313-37	(1)	(2)	21·3	21·7	1021	1056	60·9	16·8	15·5	6·5	0·3	(1)	
313-110	(1)	(2)	20·5	19·8	1003	1005	61·3	14·4	12·3	11·8	0·2	(3)	
314-2	(1)	(1)	22·6	20·3	1111	1109						(1)	cp, op
314-74	(1)	(2)	18·9	20·3	1005	1106	66·2	18·7	9·3	4·9	0·8	(3)	cp
314-580	(1)	(2)	20·5	20·7	1062	1103	64·8	15·5	11·8	7·3	0·6	(3)	cp
Composite xenoliths; garnet (G), spinel–garnet (SG) and spinel (S) zones for xenolith 113													
113G	(2)	(2)	20·2		1062		66·4	9·9	3·3	20·2		(1)	
113SG	(2)	(2)	18·8		1046		70·2	8·6	13·3	7·6		(1)	
113S	(2)	(2)	/19/		1055		68·8	22·8	6·3		2·1	(1)	
313-4	(2)	(2)	18·3		1006		52·2	14·1	14·4	19·3		(1)	
Spinel peridotites (SP-1)													
314-56	(1)	(2)	/15/		892	871	58·4	19·4	19·2		3·0	(3)	cp
314-58	(1)	(2)	/15/		874	854	62·3	18·8	15·7		3·2	(3)	cp
Spinel peridotites (SP-2)													
314-5	(2)	(2)	/15/		994		77·7	20·0	1·6		0·7	(1)	
314-6	(1)	(2)	/15/		986	1022	70·4	22·8	5·7		1·1	(1)	
314-59	(1)	(2)	/15/		1012	1054	62·0	17·0	18·8		2·2	(3)	cp
314-71	(1)	(1)	/15/		1065	1113	66·4	26·8	5·6		1·2	(1)	cp
314-72	(1)	(1)	/15/		992	1021	58·1	31·1	9·5		1·3	(1)	cp
314-73	(1)	(1)	/15/		1123	1115	62·4	23·4	13·0		1·2	(1)	cp, op

Data sources for chemical compositions: (1) this study; (2) Ionov *et al*. (1993); (3) Ionov *et al*. (in preparation). Ol, olivine; Op, orthopyroxene; Cp, clinopyroxene; Gr, garnet; Sp, spinel; Phl, phlogopite. Equilibration pressures (*P*) are after Nickel & Green (1985), temperatures (*T*) are after Brey & Köhler (1990). The *P*–*T* estimates were calculated separately for cores and rims of minerals. *T* values for spinel peridotites were calculated with $P = 19$ kbar for 113S (same as 113SG) and $P = 15$ kbar for all other samples (numbers with oblique lines before and after). Modal abundances were calculated by mass balance of mineral and whole-rock compositions. Modal compositions are not reported for 314-2 because of very heterogeneous mineral compositions.

Garnet lherzolite is the most common rock type (Fig. 2a and b). These rocks contain 6–13 wt % of garnet, 10–16% of clinopyroxene and no spinel (except rare inclusions in olivine and garnet). Garnet grains are usually large and many of them contain abundant inclusions of olivine and pyroxenes (Fig. 2b and h). Ionov *et al.* (1993) concluded from these and other observations that the garnets grew at the expense of spinel and pyroxenes (probably owing to a fall in temperature) as a result of the reaction

$$\mathrm{Sp} + \mathrm{En} + \mathrm{Di} \leftrightarrow \mathrm{Fo} + \mathrm{Gross} + \mathrm{Py}$$
$$(\text{or } \mathrm{Sp} + \mathrm{Opx} + \mathrm{Cpx} \leftrightarrow \mathrm{Ol} + \mathrm{Gar}). \quad (1)$$

Garnet–spinel peridotites differ from garnet peridotites primarily by the ubiquitous presence of spinel, both as inclusions in minerals and interstitially (Fig. 2g). The abundance of garnet varies from trace amounts to ~10%; shape and size (both between xenoliths and within individual samples) ranges from small anhedral interstitial grains to large equant grains. Garnet grains commonly have kelyphitic material along rims and cracks (Fig. 2). The kelyphite rims consist of an amorphous inner layer and a fine-grained outer layer. Garnet has been nearly completely replaced by kelyphite and spinel–orthopyroxene aggregates in some garnet–spinel xenoliths (Fig. 2d), probably because of a rise in temperature (see below).

Two types of spinel peridotites are identified here based on textures as well as equilibration temperatures and clinopyroxene abundances. The first one (SP-1) has a typical protogranular texture, with anhedral and unstrained minerals, common spinel–pyroxene intergrowths and no preferred mineral orientation. The second type (SP-2) has subhedral, elongated, commonly strained, olivine grains with slight to moderate preferred orientation (Kern *et al.*, 1996). The appearance of these rocks in thin section is similar to that of garnet-free domains in the garnet–spinel peridotites (Fig. 2a). SP-2 peridotites are further characterized by higher equilibration temperatures and generally lower modal per cent clinopyroxene than SP-1 rocks (see next section).

Two garnet-bearing xenoliths are heterogeneous (Table 1; Ionov *et al.*, 1993). 313-4 is composed mainly of garnet lherzolite, which grades into a more olivine-poor, garnet-rich rock on one side (Fig. 2c). Its bulk-rock analysis may represent a mixture of the two rock types. Xenolith 313-113 consists of spinel (113S), garnet–spinel (113SG) and garnet (113G) lherzolite parts, with gradational contacts (Fig. 2e–h). The three parts were sampled and analysed separately.

Glaser *et al.* (1999) identified 'two texturally distinguishable generations' of clinopyroxene in the Vitim xenoliths. The first one consists of equant and xenomorphic grains (0·2–2 mm); the second generation consists of irregular interstitial crystals that may form continuous networks and poikilitic grains. Glaser *et al.* attributed the second type to crystallization from a hypothetical alkaline silicate melt that infiltrated the rocks shortly before their transport to the surface. I concur with those workers that the shape and size of clinopyroxene grains in the Vitim xenoliths vary greatly and that interstitial and poikilitic clinopyroxene is locally present (Fig. 2b). However, these morphological variations are continuous and provide no evidence for the existence of two distinct grain generations. The shape and size of other minerals also vary. Garnet, in particular, commonly forms vermicular, interstitial grains in garnet–spinel peridotites (Fig. 2). These textural features are consistent with changing mineral proportions as a result of reaction (1) in response to the changes in P–T. It is also possible that slow local recrystallization in the presence of fluid or melt may result in the formation of interconnected poikilitic networks of pyroxene. By comparison, there is no petrographic evidence for rapid crystallization of interstitial pyroxene in a recent metasomatic event. Furthermore, the preservation of cryptocrystalline kelyphite rims in adjacent garnet argues against such a process. Moreover, such a process does not appear to be plausible in terms of textural and phase relations, as well as mineral compositions, at appropriate P–T conditions and melt compositions.

Less than 10% of the xenoliths analysed in this study contain accessory amphibole and phlogopite. These minerals are uncommon in the Vitim peridotites and usually occur in pyroxenites and pyroxene-rich veins in peridotites. Some xenoliths have alteration products, commonly as cryptocrystalline material along grain boundaries and cracks (Fig. 2a, b and h). Electron microprobe analyses (e.g. sample 313-37) and X-ray diffraction data obtained on intergranular material separated from one of the xenoliths indicate that it may contain zeolites.

MAJOR ELEMENT COMPOSITIONS

Bulk rocks

Major element analyses of Vitim xenoliths obtained in this study are listed in Table 2. These results, together with the data published previously (Ionov *et al.*, 1993), are illustrated in Fig. 3. Plotted for comparison in Fig. 3 are data for peridotite xenoliths from Tariat (central Mongolia; Fig. 1) and for peridotites from the Horoman massif in Japan (Takazawa *et al.*, 2000). The Tariat xenoliths are generally fertile (Press *et al.*, 1986; D. Ionov, unpublished data, 2000). The Horoman

peridotites range from moderately to strongly depleted in basaltic components, consistent with an origin as residues of different degrees of polybaric partial melting from a primitive mantle source (Takazawa *et al.*, 2000).

High contents of CaO (usually >2·5%) and Al_2O_3 (usually >2·8%) characterize the majority of Vitim peridotites as fertile and are consistent with typically high modal per cent clinopyroxene and garnet (Table 1). Moreover, the contents of Ca and Al in several Vitim

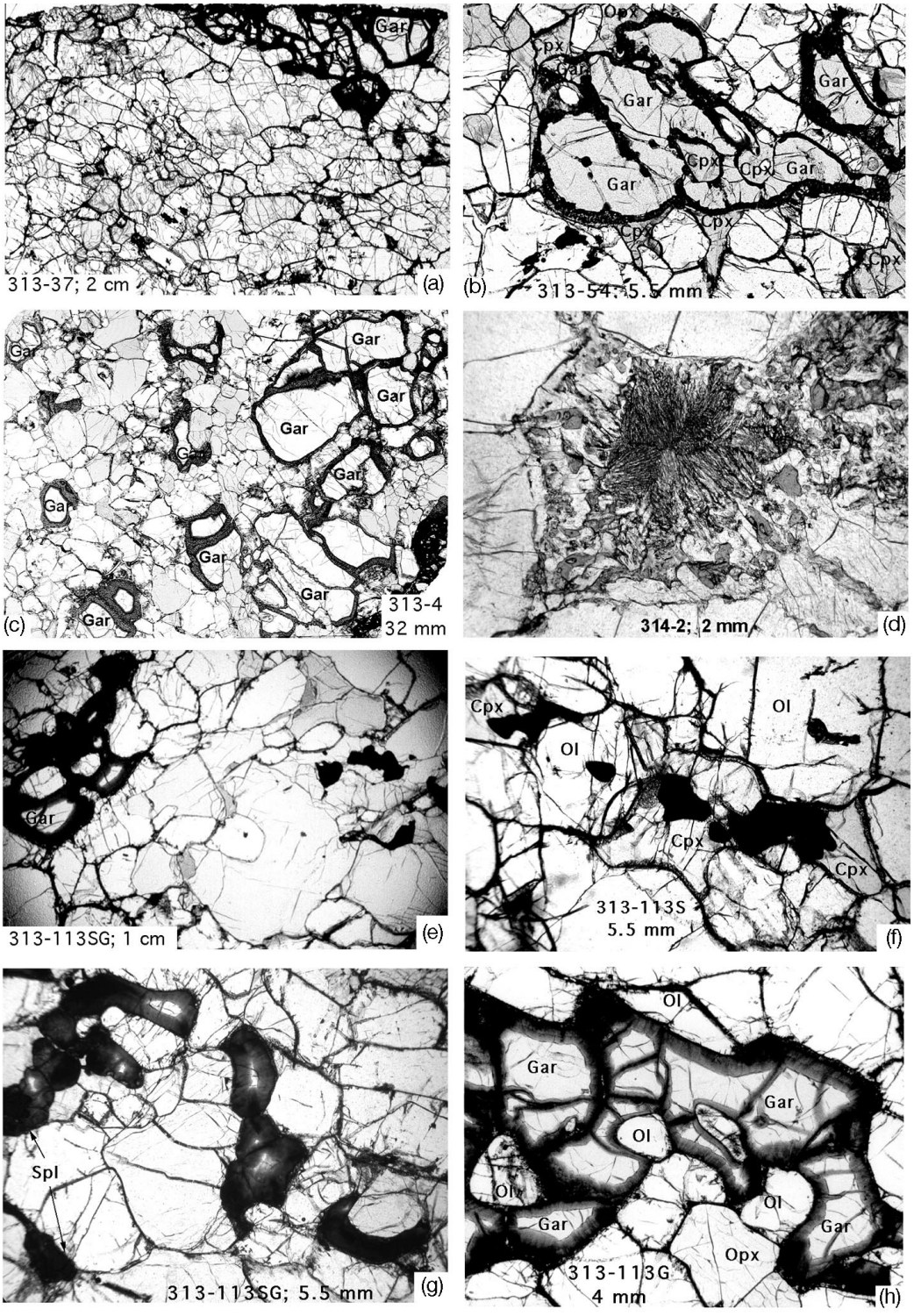

xenoliths are higher than those normally inferred for the primitive mantle (Hart & Zindler, 1986; Hofmann, 1988). The few samples with relatively low Ca and Al are spinel peridotites. As noted earlier by Ionov *et al.* (1993), the generally fertile Vitim xenolith suite is fundamentally different in terms of major element and modal compositions from the typically depleted garnet and spinel peridotite xenoliths in kimberlites from the nearby Siberian craton (Fig. 3) and other cratons (Boyd, 1989; Boyd *et al.*, 1997; Schmidberger & Francis, 1999; Pearson *et al.*, 2003). The average composition of the Vitim xenoliths is similar to averages for other xenolith suites (mostly consisting of spinel peridotites) from the Baikal region and central Mongolia (Ionov, 2002). Taken together, these xenolith suites appear to outline a large-scale fertile lithospheric mantle domain south of the Siberian craton.

The fertile Vitim peridotites form a relatively broad field on the CaO–Al_2O_3 co-variation plot (Fig. 3a). Furthermore, the majority of fertile garnet-bearing Vitim lherzolites have higher Al_2O_3 at a given MgO than the Tariat xenoliths and clearly plot above the upper end of the combined Tariat–Horoman MgO–Al_2O_3 trend (Fig. 3b). By contrast, the Tariat and Horoman peridotites define more narrow fields (and yield higher correlation coefficients, Fig. 3). The differences in Mg–Al relationships and the poorer correlations between Ca and Al and some other major oxides for the Vitim xenolith suite are not likely to be due to analytical problems. First, the analyses from this study (Table 2) were obtained in the same laboratory (Niigata) and using the same method as applied to the Tariat peridotites, which have a similar range of Mg, Ca and Al. Second, the data from Ionov *et al.* (1993) are averages of two duplicates; the differences between the duplicate analyses of each xenolith are much smaller than the range of Ca values at a given Al and vice versa in Fig. 3a. An alternative explanation could be that some of the xenoliths from the earlier study (Ionov *et al.*, 1993) were too small to provide representative samples of these coarse-grained rocks if their minerals are unevenly distributed on a millimetre–centimetre scale (Fig. 2a, c and e) (Boyd *et al.*, 1997). However, several 'anomalous' compositions were obtained on large ($\geq$0·5 kg) samples from this study (313-102, 313-112, 313-240) and therefore should be considered as representative.

Mineral compositions and P–T estimates

EPMA data for representative spinel and garnet lherzolites are given in Table 3. The complete dataset is available as an electronic appendix, which can be downloaded from http://www.petrology.oupjournals.org. The EPMA data reported here are usually based on larger numbers of individual analyses for each mineral than those reported for the same samples by Ionov *et al.* (1993). Furthermore, the data in this study are reported separately for cores of pyroxene grains with different textural position and size (large, medium and small) if their compositions are different. Pressure (P) and temperature (T) estimates are given in Table 1. Mineral compositions and P–T estimates obtained in this study correspond broadly to the results of Ashchepkov (1991), Ionov *et al.* (1993) and Glaser *et al.* (1999). Only selected aspects of these data, which are relevant to this study, are considered here.

Pyroxenes are chemically zoned in many xenoliths. The contents of Al and Cr in pyroxenes from SP-1 spinel peridotites decrease from core to rim; the content of Ca decreases towards the rim in orthopyroxene and increases in clinopyroxene. These trends are consistent with incomplete diffusional inter-mineral exchange caused by falling ambient temperatures (Brey & Köhler, 1990). By contrast, pyroxenes from SP-2, garnet and garnet–spinel peridotites typically have higher Al and Cr towards the rim; the content of Ca increases towards the rim in orthopyroxene and in clinopyroxene. These differences may also exist between the cores of large and small pyroxene grains (Table 3). 'Poikilitic' clinopyroxene in garnet peridotites has higher Al contents than rims of normal clinopyroxene grains in some samples, with no systematic differences for other elements (313-240, Table 3). Garnet grains

Fig. 2 (opposite). (a–h) Photomicrographs of Vitim peridotite xenoliths in plane-polarized transmitted light. Sample numbers and the width of the field of view along the long axis are indicated on each photograph. Ol, olivine; Opx, orthopyroxene; Cpx, clinopyroxene; Gar, garnet; Spl, spinel. (a) Irregular distribution of garnet grains in garnet lherzolite 313-37. [Note a cluster of irregularly shaped garnet grains (with dark kelyphite along rims and cracks, upper right) and lack of garnet in the rest of the section.] Dark material inside some mineral grains is alteration products; host volcanic material is locally present, together with alteration products, along grain boundaries. (b) Garnet–pyroxene relationships in garnet lherzolite 313-54. Garnet grains have complex shapes; clinopyroxene occurs as 'poikilitic' grains next to garnet and as inclusions in garnet. Dark secondary alteration products inside olivine (lower left) should be noted. (c) Irregular garnet distribution in composite xenolith 313-4 containing a garnet-rich, olivine-poor zone (right). (d) Opx–Spl aggregates replacing a previously existing garnet grain in xenolith 314-2 as a result of a temperature rise. Small garnet relics are locally preserved elsewhere in this xenolith. (e) Transition zone between garnet–spinel (left) and spinel (right) peridotite in composite xenolith 313-113. (f) Spinel lherzolite in composite xenolith 313-113. Spinel (and no garnet) both along grain boundaries and inside olivine and pyroxene should be noted. (g) Garnet–spinel lherzolite in composite xenolith 313-113. Small, anhedral garnet grains are interstitial and coexist with spinel. (h) Garnet lherzolite zone of composite xenolith 313-113. Garnet grains are irregular and contain abundant equant olivine inclusions. Host volcanic material (black, with small vugs), mainly along kelyphitized garnet rims and cracks, should be noted.

Table 2: Whole-rock XRF analyses

Rock:	Garnet peridotites						Gar–Spl peridotite	Spinel peridotites		
Sample:	313-102	313-104	313-106	313-112	313-240	313-241	314-2	314-71	314-72	314-73
SiO_2	43·55	45·08	44·24	44·92	43·96	44·18	44·41	44·22	44·77	44·34
TiO_2	0·14	0·17	0·15	0·15	0·12	0·15	0·24	0·16	0·12	0·24
Al_2O_3	4·48	3·66	3·33	4·17	3·25	3·62	3·38	2·18	2·80	2·87
Cr_2O_3	0·36	0·35	0·37	0·36	0·34	0·36	0·39	0·40	0·35	0·39
ΣFeO	8·62	8·24	8·43	8·26	8·63	8·58	8·23	8·23	8·12	9·30
MnO	0·15	0·14	0·13	0·14	0·13	0·13	0·13	0·13	0·13	0·13
NiO	0·22	0·24	0·26	0·24	0·25	0·25	0·26	0·29	0·27	0·27
MgO	36·73	38·21	39·44	38·58	40·15	39·39	39·91	42·84	40·81	39·56
CaO	3·56	3·59	3·13	2·90	2·82	2·97	2·73	1·40	2·14	2·61
Na_2O	0·33	0·36	0·31	0·26	0·25	0·39	0·24	0·11	0·25	0·24
K_2O	0·02	0·03	0·02	0·02	0·03	0·00	0·10	0·02	0·03	0·04
P_2O_5	0·02	0·02	0·02	0·01	0·02	0·00	0·03	0·02	0·02	0·02
Total	98·17	100·09	99·84	100·01	99·95	100·01	100·05	99·98	99·79	99·99
Mg no.	0·884	0·892	0·893	0·893	0·892	0·891	0·896	0·903	0·900	0·884
Ca/Al	1·07	1·33	1·27	0·94	1·17	1·11	1·09	0·87	1·03	1·23

Total iron is shown as FeO. Mg number = molar MgO/(MgO + FeO). Analyses of other Vitim xenoliths have been given by Ionov *et al.* (1993).

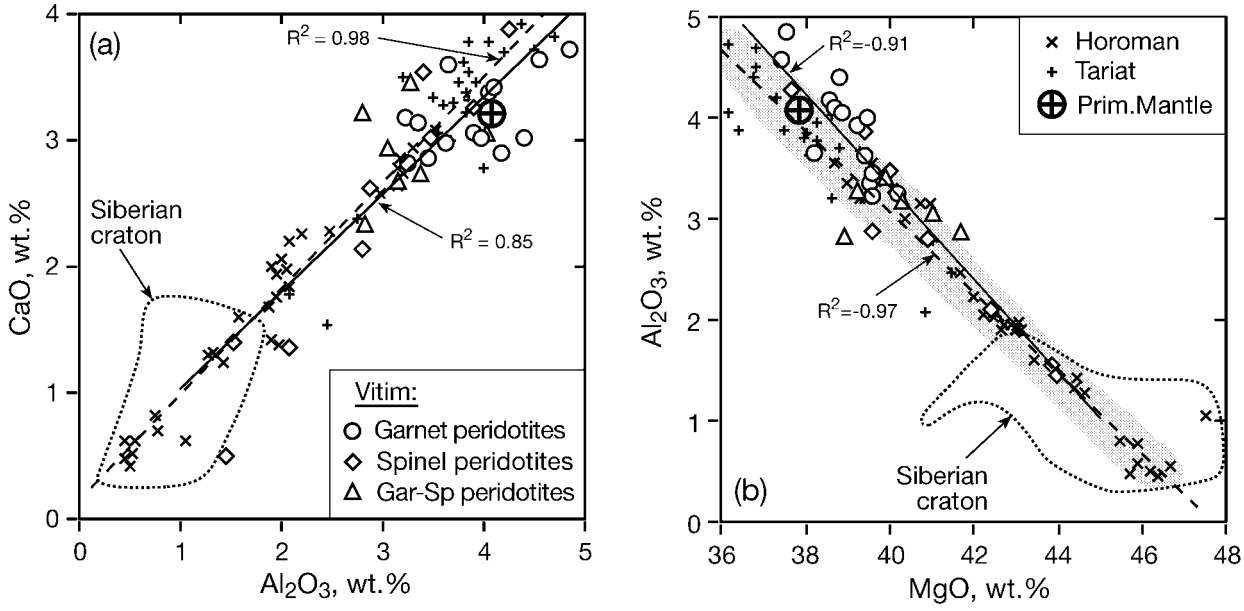

Fig. 3. Co-variation plots of Al_2O_3 vs CaO (a) and MgO (b) for the Vitim peridotite xenoliths [data from this study and Ionov *et al.* (1993)]. Also shown are peridotites from the Horoman massif, Japan (Takazawa *et al.*, 2000) and peridotite xenoliths from Tariat, Mongolia (D. Ionov, unpublished data, 2000). Dashed line contours the field of peridotite xenoliths from the Udachnaya kimberlite pipe on the Siberian craton [≥90% of samples from Boyd *et al.* (1997)]. Grey area in (b) contours the combined field of the Tariat and Horoman peridotites (drawn visually to exclude apparent outliers). Linear regression trends (continuous lines for the Vitim suite; dashed lines for the combined Tariat and Horoman suite; R^2, correlation coefficients) show that Vitim lherzolites tend to have higher Al at given Mg. All analyses are recalculated to 100% total, with all Fe as FeO. Primitive mantle composition is after Hart & Zindler (1986).

Table 3: Major element compositions of minerals in representative xenoliths

Sample:	313-102, garnet lherzolite										314-58, low-*T* spinel lherzolite							
Mineral:	Ol c.	Op c.	Op c.	Op rim	Cp c.	Cp rim	Gr c.	Gr int	Gr rim	Sp	Ol c.	Op c.	Op c.	Op rim	Cp c.	Cp c.	Cp rim	Sp c.
Size:		low-Ca										v.large	med		large	small		
n:	av. 2	av. 2	av. 3	av. 2	av. 5	av. 4	av. 4		av. 4		av. 3	av. 4	av. 4	av. 3	av. 3	av. 3	av. 2	av. 3
SiO_2	40·65	55·39	54·95	54·49	52·37	52·03	42·01	41·84	42·31	0·14	40·75	54·32	54·74	55·68	51·69	51·82	52·38	0·04
TiO_2	0·02	0·14	0·12	0·18	0·51	0·51	0·20	0·16	0·21	0·25	0·02	0·16	0·14	0·07	0·63	0·66	0·54	0·05
Al_2O_3	0·05	3·77	4·45	5·12	5·99	6·86	23·48	23·42	23·52	54·79	0·02	5·14	4·82	3·52	7·28	7·03	5·86	57·73
Cr_2O_3	0·02	0·56	0·32	0·57	1·13	1·06	1·05	1·15	1·28	10·93	0·00	0·39	0·35	0·21	0·71	0·74	0·58	8·72
FeO*	10·26	6·19	6·37	6·43	3·39	3·55	7·61	7·50	7·41	11·85	10·17	6·55	6·66	6·47	2·53	2·45	2·56	11·43
MnO	0·13	0·14	0·12	0·11	0·05	0·08	0·30	0·28	0·28	0·00	0·13	0·13	0·13	0·11	0·05	0·10	0·07	0·00
MgO	49·62	33·27	33·12	32·65	16·42	16·34	21·35	21·42	21·76	20·56	49·31	32·79	33·09	33·75	14·12	14·16	14·85	20·32
CaO	0·11	0·84	0·97	1·16	18·61	17·96	5·02	4·97	5·03	0·00	0·01	0·45	0·44	0·40	20·72	20·75	21·21	0·00
Na_2O	0·02	0·18	0·20	0·20	1·75	1·82	0·03	0·03	0·02	0·02	0·01	0·05	0·06	0·05	1·98	1·97	1·69	0·01
NiO	0·39	0·15	0·11	0·11	0·07	0·05	0·01	0·00	0·01	0·36	0·34	0·05	0·09	0·09	0·03	0·02	0·06	0·37
Total	101·27	100·64	100·74	101·01	100·29	100·27	101·06	100·78	101·82	98·90	100·76	100·03	100·52	100·36	99·75	99·71	99·79	98·67
Mg no.	0·896	0·905	0·903	0·901	0·896	0·891	0·833	0·836	0·840	0·756	0·896	0·899	0·899	0·903	0·909	0·911	0·912	0·760

Sample:	313-106, garnet lherzolite										314-71, high-*T* spinel lherzolite							
Mineral:	Ol c.	Op c.	Op c.	Op rim	Cp c.	Cp c.	Cp rim	Gr c.	Gr rim	Sp	Ol c.	Op c.	Op c.	Op rim	Cp c.	Cp c.	Cp rim	Sp c.
Size:		large	small		large	med.		large				large	med		large	small		
n:	av. 4	av. 3	av. 6	av. 2	av. 3	av. 2	av. 3	av. 8	av. 3	av. 4	av. 4	av. 6	av. 6	av. 5	av. 3	av. 2		av. 2
SiO_2	40·56	54·71	54·67	54·30	51·90	52·02	52·11	41·88	41·72	0·09	40·49	54·44	54·07	53·79	51·66	51·37	50·89	0·13
TiO_2	0·01	0·18	0·18	0·19	0·64	0·66	0·60	0·18	0·20	0·31	0·01	0·11	0·22	0·32	0·39	0·70	0·88	0·82
Al_2O_3	0·03	3·86	4·11	4·49	6·10	5·98	6·15	22·83	22·63	50·90	0·05	4·53	4·83	5·18	5·70	6·24	6·72	43·24
Cr_2O_3	0·06	0·56	0·55	0·56	1·03	1·17	1·27	1·00	1·25	14·28	0·05	0·71	0·67	0·68	1·19	1·28	1·11	20·13
FeO*	9·85	6·03	6·15	6·07	2·93	3·09	3·17	7·48	7·47	12·09	8·79	5·61	5·68	5·59	3·13	3·38	3·55	12·49
MnO	0·10	0·14	0·13	0·13	0·09	0·07	0·07	0·32	0·32	0·00	0·14	0·10	0·09	0·12	0·08	0·09	0·12	0·00
MgO	48·80	32·76	32·44	32·18	15·12	15·28	15·32	20·80	20·79	19·70	49·37	32·40	32·19	31·95	16·33	16·12	16·14	19·55
CaO	0·09	0·78	0·87	0·87	18·94	18·83	18·43	4·82	4·92	0·02	0·10	1·04	1·15	1·23	18·28	17·91	17·61	0·01
Na_2O	0·01	0·17	0·17	0·18	1·97	1·97	2·00	0·03	0·03	0·00	0·02	0·17	0·19	0·19	1·49	1·59	1·64	0·01
NiO	0·41	0·10	0·11	0·11	0·03	0·02	0·05	0·03	0·04	0·35	0·37	0·10	0·13	0·10	0·05	0·08	0·06	0·40
Total	99·91	99·28	99·38	99·07	98·74	99·10	99·16	99·36	99·36	97·74	99·39	99·21	99·22	99·13	98·29	98·75	98·72	96·78
Mg no.	0·898	0·906	0·904	0·904	0·902	0·898	0·896	0·832	0·832	0·744	0·909	0·911	0·910	0·911	0·903	0·895	0·890	0·736

usually have higher Cr at the rims than inside the grains. P–T estimates in Table 1 were calculated separately from analyses of cores of large grains and from rim analyses.

Temperature estimates (Ca-opx thermometer, Brey & Köhler, 1990) for mineral cores in garnet-bearing peridotites range from 950 to 1110°C; pressures (Nickel & Green, 1985) range from 18 to 23 kbar (Fig. 4). The P–T trend obtained for garnet-bearing peridotites in this study (Fig. 4) is poorly defined, probably because of widespread mineral zoning. Moreover, construction of a local geotherm requires data for shallower garnet pyroxenites (Litasov *et al.*, 2000). Temperatures for SP-2 peridotites (990–1120°C) overlap the T range for the garnet-bearing peridotites and are much higher than for SP-1 peridotites (<900°C). Assuming that temperature gradually rises with depth, the SP-1 peridotites are from the shallow mantle, probably above the depth of the spinel–garnet facies transition for fertile peridotites (Fig. 4). It follows also that

Table 3: continued

Sample:	313-240, garnet lherzolite											314-72, medium-*T* spinel lherzolite					
Mineral:	Ol c.	Op c.	Op c.	Op rim	Cp c.	Cp c.	Cp rim	Cp oik	Gr c.	Gr rim	Sp	Ol c.	Op c.	Op rim	Cp c.	Cp rim	Sp c.
Size:		large	small		large	med.		at Gr			in Gr						
n:	av. 3	av. 5	av. 4	av. 2	av. 6	av. 5	av. 2		av. 4	av. 3	av. 2	av. 4	av. 5	at cp	av. 3		av. 2
SiO_2	40·48	55·11	54·77	53·94	51·77	52·22	52·35	52·00	42·05	42·28	0·13	40·40	54·25	53·67	51·56	51·15	0·12
TiO_2	0·02	0·17	0·17	0·17	0·57	0·53	0·52	0·53	0·17	0·19	0·34		0·13	0·15	0·48	0·42	0·22
Al_2O_3	0·05	3·97	4·74	5·06	5·70	6·08	6·68	7·05	22·88	22·82	47·40		4·79	5·00	6·43	6·73	53·65
Cr_2O_3	0·03	0·58	0·62	0·68	1·15	1·24	1·33	1·26	1·16	1·41	18·37		0·44	0·47	0·96	0·89	13·48
FeO*	9·76	6·25	6·21	6·08	3·14	3·25	3·37	3·64	7·26	7·02	12·66	9·72	6·10	6·08	2·99	3·20	11·42
MnO	0·14	0·13	0·15	0·14	0·06	0·07	0·06	0·14	0·30	0·25	0·00	0·13	0·13	0·11	0·07	0·06	0·00
MgO	49·32	33·09	32·42	32·06	15·68	16·09	16·28	16·03	21·32	21·54	19·25	50·06	33·50	33·29	15·92	15·92	20·73
CaO	0·08	0·81	1·07	1·18	19·00	18·23	17·63	17·84	5·00	4·92	0·01	0·08	0·78	0·87	19·66	19·41	0·01
Na_2O	0·02	0·17	0·20	0·21	1·82	1·78	1·83	1·88	0·03	0·02	0·01		0·12	0·17	1·65	1·62	0·00
NiO	0·44	0·10	0·12	0·11	0·06	0·08	0·07	0·10	0·04	0·01	0·24	0·38	0·11	0·13	0·05	0·06	0·36
Total	100·34	100·38	100·48	99·63	98·95	99·56	100·11	100·45	100·21	100·44	98·41	100·78	100·36	99·95	99·96	99·48	99·99
Mg no.	0·900	0·904	0·903	0·904	0·899	0·898	0·896	0·887	0·840	0·846	0·731	0·902	0·907	0·907	0·905	0·899	0·764

C., core; int., intermediate (between core and rim); oik, oikocrystals (poikilitic Cp); av., average; *n*, number of analyses.

SP-2, garnet–spinel and garnet peridotites coexist (e.g. are interlayered) in the depth range ~60–75 km (18–23 kbar).

When minerals are zoned their rims may approach chemical equilibrium at ambient P–T conditions whereas their cores retain compositions corresponding to previous P–T conditions because of slow diffusional exchange (Stern *et al.*, 1999). Pyroxene zoning indicates that SP-1 peridotites equilibrated under conditions of slow cooling. The other rock types, situated at greater depths, experienced recent heating (also indicated by local breakdown of garnet to form kelyphite and pyroxene–spinel intergrowths, Fig. 2d). Differences in mineral zoning patterns and kelyphite abundances between xenoliths indicate that heating regimes may have varied locally; it is not clear whether the heating degree generally increased with depth.

TRACE ELEMENT COMPOSITIONS

Laser-ablation–ICP-MS analyses of minerals

LA–ICP-MS trace element analyses of minerals are given in Table 4 and illustrated in Fig. 5. A common feature of the REE patterns of clinopyroxene from all rock types is a continuous decrease of primitive mantle-normalized (REE_N) abundances from Sm to La (Fig. 5a and c). Furthermore, normalized abundances of Th, U and Nb are much lower than those of La and in most cases show a continuous decrease from La to Th (Fig. 5b and d). These patterns show no apparent evidence for metasomatic addition of incompatible elements (e.g. LREE enrichment); therefore, they may represent residues produced by partial melting. On the other hand, clinopyroxenes in several spinel and garnet–spinel xenoliths (shown with grey symbols and lines in Fig. 5a and c) have higher LREE and Sm abundances than clinopyroxene in the most fertile spinel and garnet lherzolites (e.g. 314-56). The mismatch between the relatively high LREE contents in these samples and their moderately depleted major element compositions and modal mineralogy is not consistent with partial melting relationships and may indicate re-equilibration of these initial melting residues with evolved liquids, i.e. the presence of a minor metasomatic component in their LREE patterns.

The distribution of MREE and HREE (from Eu to Lu) in the clinopyroxenes follows three main patterns, which can be roughly correlated with rock type (Fig. 5a and c): (1) clinopyroxenes from the SP-1 samples and one SP-2 sample (314-59) have nearly flat MREE–HREE patterns; (2) REE_N values in clinopyroxenes from three SP-2 peridotites and one garnet–spinel peridotite decrease continuously from Eu (~3–5) to Lu (1·3–2); (3) clinopyroxenes from all garnet peridotites and one garnet–spinel peridotite share a common trend of continuously decreasing primitive mantle-normalized values from Eu (~3–4) to Yb and Lu

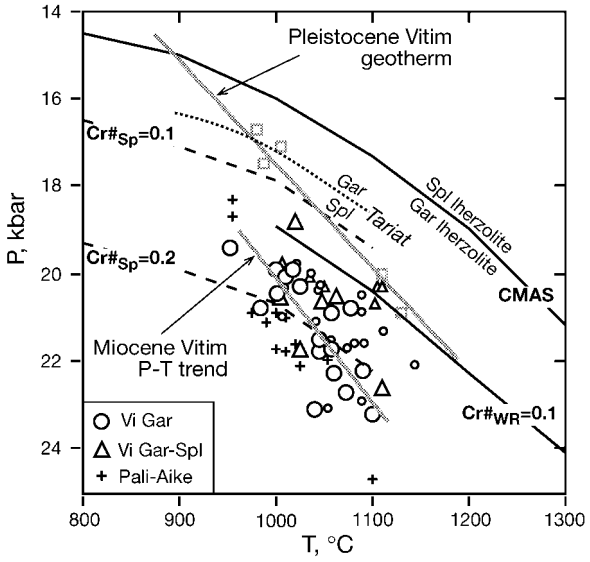

Fig. 4. *P–T* estimates for the Vitim garnet-bearing xenoliths (open circles and triangles) using the Ca-in-opx thermometer of Brey & Köhler (1990) combined with barometer of Nickel & Green (1985). Large and small symbols show *P–T* values for mineral cores and rims, respectively. Grey squares are *P–T* estimates for xenoliths from young (<5 Ma) Vitim basalts (Ionov *et al.*, 1993), grey line is a *P–T* trend for a larger set of Pleistocene Vitim xenoliths (Ashchepkov *et al.*, 1989; Litasov *et al.*, 2000; Ionov, 2002). Black crosses are *P–T* estimates for xenoliths from Pali-Aike, Patagonia (Stern *et al.*, 1986; Kempton *et al.*, 1999*b*) calculated for mineral cores using the same methods. Vitim xenoliths with lowest *T* values (at a given *P*) plot close to the Pali-Aike *P–T* trend. Continuous black lines are transition boundaries between spinel and garnet lherzolites in the CMAS system (Klemme & O'Neill, 2000) and for a lherzolite with whole-rock Mg number = 0·9 and Cr number = 0·1 (Nickel, 1986). Dashed lines are spinel-to-garnet transition boundaries as a function of Cr/(Cr + Al) ratios in spinel (at whole-rock Mg number of 0·9) (O'Neill, 1981). Dotted line is a spinel–garnet phase transition boundary established for fertile lherzolites from Tariat, Mongolia (Ionov *et al.*, 1998).

(0·2–0·5). Importantly, the HREE–MREE patterns of clinopyroxenes from garnet peridotites and from many SP-2 peridotites are similar, except that the downward Eu–Lu trend is steeper for the former. The SP-2 peridotites contain no garnet, yet their clinopyroxenes have a 'garnet signature' in their REE patterns, with much lower HREE abundances than in clinopyroxenes from SP-1 rocks.

REE data on minerals from Vitim xenoliths obtained in other studies confirm the important, but seemingly contradictory, finding of this study that HREE abundances in clinopyroxenes from some garnet-free peridotites are very low and may indicate equilibration with garnet. Clinopyroxenes from all three spinel peridotites analysed by Glaser *et al.* (1999) and V. Salters (personal communication, 2002) have even lower HREE than those for SP-2 peridotites in this study and overlap the HREE range determined for clinopyroxenes from garnet-bearing rocks (Fig. 6). Therefore, the HREE-poor clinopyroxenes are not limited to rare exotic samples, but are common in some Vitim spinel peridotites. Importantly, equilibration temperatures (and therefore depth of origin) in these spinel peridotites (SP-2) overlap with *T* estimates for garnet-bearing peridotites. Furthermore, Kempton *et al.* (1999*b*) found HREE depletions in several spinel peridotites from Pali-Aike, which appear to come from the same depth range as garnet-bearing xenoliths (Fig. 4).

REE patterns of most garnets are nearly flat from Lu to Dy (at 7–10 × primitive mantle). In two samples analysed by LA–ICP-MS (313-102, 313-104), garnets have much higher Lu and Yb (~20 × primitive mantle) and fractionated HREE patterns (Fig. 5e). INAA data reported by Ionov *et al.* (1993) show high Lu (≥1 ppm) and Yb (≥5 ppm) also in garnets from samples 313-8, 313-37 and 313-113G. In contrast to the broad variations in HREE (from Lu to Dy), all garnets have similar MREE–LREE, Ti and Sr abundances, with a steep decline from Tb to La, and negative anomalies for Ti and Sr (Fig. 5f). Zr abundances in coexisting garnet and clinopyroxene are generally similar except for the two HREE-rich garnets, which contain nearly twice as much Zr as coexisting clinopyroxene (Fig. 5). By contrast, Hf abundances are higher in clinopyroxenes than in garnets. As a result, Zr/Hf values in garnets are much higher (>primitive mantle) than in coexisting clinopyroxenes (<primitive mantle), consistent with experimental studies (Fujinawa & Green, 1997; Salters & Longhi, 1999; Klemme et al., 2002).

Trace element zoning in garnet and clinopyroxene

The laser-ablation analyses of garnet and clinopyroxene reported in the previous section were obtained on cores of mineral grains. Trace elements were also determined in thin section by SIMS in core–rim profiles across garnet and clinopyroxene grains in one xenolith with HREE-rich garnet (313-102, Fig. 5e) and one xenolith with normal HREE concentrations in garnet (313-54; Ionov et al., 1993). The SIMS analyses are given in Table 5 and illustrated in Fig. 7.

Garnet in xenolith 313-54 is not zoned. In particular, the Lu and Yb abundances are identical in its core and rim. By contrast, Lu and Yb abundances in the core of the garnet grain analysed in xenolith 313-102 (1200 μm across) are more than twice as high as in its rim. The low HREE values were obtained both at the rim of the garnet and in two more spots located ~100 and ~200 μm from the rim. The SIMS data indicate that the high HREE content of this garnet, analysed by LA–ICP-MS, is typical of only its central part.

Table 4: LA-ICPMS analyses of minerals (ppm)

Rock:	Garnet lherzolites																Garnet–spinel lherzolites				Spinel lherzolite					
Sample:	313-6			313-102		313-104		313-106		313-112		313-240		313-241			314-2		314-74	314-580	314-58	314-59	314-71	314-72	314-73	
Mineral:	Cpx	Opx	Gar	Cpx	Gar	Cpx	Gar	Cpx	Gar	Cpx	Gar	Cpx	Gar	Cpx	Gar		Cpx	Opx	Cpx	Cpx	Cpx	Cpx	Cpx	Cpx	Cpx	Opx
n:			av. 2		av. 2		av. 2		av. 2		av. 2		av. 2		av. 2							av. 2	av. 2	av. 2		
Sc	27	8	96	30	99	31	88	30	88	29	88	30	101	31	95		38	12	53	29	64	60	51	51	31	12
Ti	3419	972	1064	2934	966	3228	1143	3526	1134	3379	1066	3184	1114	3518	1135		3422	854	1495	3040	3571	2223	2161	2252	5049	1686
V	345	113	104	331	97	330	99	350	100	341	98	334	97	347	104		273	105	254	293	281	255	225	231	249	111
Cr				6935		7304		8781		8189		8626		8041					6504	6365	5115	6164	7970	5159	6777	3656
Co	24	63	44	26	45	26	44	23	44	24	45	25	44	26	44				26	28	18	23	26	22	33	58
Ni	392	833	65	425	65	411	66	368	63	377	57	426	66	419	72				453	407	275	386	440	350	490	772
Ga	10·1	8·2	4·5	9·3	4·2	9·3	4·4	9·5	5·4	9·0	3·8	8·7	3·6	9·6	5·6				3·8	8·7	4·1	3·7	4·2	3·9	10·9	8·5
Sr	83·1	0·46	0·21	76·4	0·15	91·1	0·14	84·1	0·15	73·3	0·10	80·6	0·14	85·8	0·22		90·2	0·44	53·8	101·6	71·7	66·3	75·2	62·3	74·9	1·07
Y	3·2	0·30	26·6	3·2	40·7	4·1	40·0	3·1	21·4	2·9	27·7	3·4	34·1	4·0	25·0		6·5	0·56	8·0	4·1	21·8	13·9	11·0	6·9	8·8	0·85
Zr	24·9	1·63	30·3	19·0	33·4	22·6	41·8	23·5	19·8	22·5	27·0	22·9	28·3	23·8	21·8		39	3·0	12·1	49·5	36·1	24·9	49·8	22·2	32·6	3·96
Nb	0·65	0·041	0·052	0·30	0·05	0·91	0·12	0·19	0·055	0·17	b.d.	0·16	0·04	0·19	0·056		0·28	0·03	0·44	0·96	0·080	0·51	0·37	0·22	0·32	b.d.
Ba	0·06	b.d.	b.d.	0·06	b.d.	b.d.	b.d.	0·051	b.d.	b.d.	0·016	0·09	b.d.	0·07	b.d.		b.d.	b.d.	0·17	0·15	0·020	0·050	0·17	0·047	0·14	b.d.
La	1·30	0·010	b.d.	0·96	0·011	1·51	b.d.	0·99	0·012	0·84	0·008	0·93	0·012	1·04	b.d.		1·38	b.d.	0·86	2·50	0·84	1·02	1·71	1·00	2·12	b.d.
Ce	4·33	0·027	0·058	3·44	0·074	4·98	0·085	3·71	0·062	3·30	0·043	3·58	0·068	4·08	0·10		5·2	0·038	2·60	8·10	3·50	3·50	6·14	3·04	6·32	0·19
Pr	0·75	b.d.	b.d.	0·60	0·025	0·82	0·027	0·66	0·028	0·66	0·026	0·64	0·024	0·73	0·045		1·00	0·006	0·42	1·32	0·59	0·56	1·06	0·53	1·14	b.d.
Nd	4·52	0·050	0·33	3·76	0·40	4·97	0·34	4·80	0·34	4·12	0·33	4·23	0·35	4·72	0·41		5·4	0·056	1·90	8·20	4·20	3·50	6·16	3·10	6·58	b.d.
Sm	1·55	0·036	0·65	1·44	0·54	1·69	0·65	1·52	0·61	1·51	0·64	1·37	0·62	1·66	0·61		1·83	0·039	0·90	2·10	1·90	1·20	2·09	1·32	2·50	b.d.
Eu	0·59	0·022	0·40	0·49	0·37	0·65	0·47	0·57	0·42	0·58	0·41	0·59	0·44	0·66	0·42		0·68	0·014	0·30	0·81	0·80	0·53	0·76	0·53	0·80	b.d.
Gd	1·46	0·031	2·07	1·37	2·09	1·54	2·07	1·52	1·54	1·40	2·12	1·46	2·26	1·68	1·77		2·05	b.d.	1·60	2·00	2·90	1·80	2·22	1·54	2·47	0·13
Tb	0·21	0·010	0·55	0·17	0·61	0·22	0·59	0·22	0·42	0·22	0·57	0·21	0·58	0·25	0·50		0·31	0·011	0·26	0·27	0·54	0·35	0·36	0·28	0·37	b.d.
Dy	0·89	0·070	4·37	0·90	5·77	1·10	5·95	0·87	3·29	0·91	4·33	0·95	5·14	1·15	4·11		1·56	0·11	1·60	1·10	4·00	2·90	2·23	1·62	2·19	b.d.
Ho	0·14	0·016	1·07	0·14	1·66	0·16	1·81	0·15	0·87	0·12	1·16	0·14	1·34	0·15	1·07		0·25	0·024	0·30	0·15	0·85	0·53	0·44	0·29	0·33	0·042
Er	0·29	b.d.	2·94	0·23	5·76	0·38	6·03	0·25	2·67	0·22	3·27	0·27	3·86	0·36	3·25		0·57	0·053	0·92	0·32	2·40	1·50	1·17	0·68	0·87	0·110
Yb	0·15	0·040	3·00	0·13	7·70	0·20	7·92	0·14	3·34	0·11	3·18	0·19	4·14	0·22	3·48		0·34	0·071	0·66	0·11	2·20	1·70	1·07	0·59	b.d.	0·12
Lu	0·018	b.d.	0·44	b.d.	1·28	b.d.	1·37	b.d.	0·55	b.d.	0·44	b.d.	0·62	0·022	0·54		0·038	0·01	0·070	0·020	0·30	0·24	0·127	0·077	0·080	b.d.
Hf	1·02	0·049	0·57	0·75	0·58	0·93	0·69	0·93	0·31	0·97	0·44	0·91	0·40	1·04	0·34		1·35	0·061	0·39	1·50	1·19	0·91	1·31	0·75	1·53	0·18
Pb	0·14	b.d.	b.d.	b.d.	b.d.	0·091	b.d.	0·19	b.d.	0·16	b.d.	0·083	b.d.	0·077	b.d.		0·11	b.d.	b.d.	0·21	b.d.	b.d.	0·101	b.d.	b.d.	0·13
Th	0·066	b.d.	b.d.	0·019	b.d.	0·104	b.d.	0·017	b.d.	b.d.	b.d.	0·017	b.d.	0·030	b.d.		0·032	0·001	0·050	0·15	0·010	0·040	0·023	0·030	0·046	b.d.
U	0·017	b.d.	b.d.	b.d.	0·007	0·022	b.d.	b.d.	b.d.	b.d.	b.d.	b.d.	b.d.	b.d.	b.d.		0·009	0·001	b.d.	0·024	b.d.	0·023	0·01	b.d.	0·011	b.d.

b.d., below detection limit; empty entries, not determined; *n*, number of analyses. Analyses of sample 314-2 were performed by A. Zanetti (Pavia, Italy).

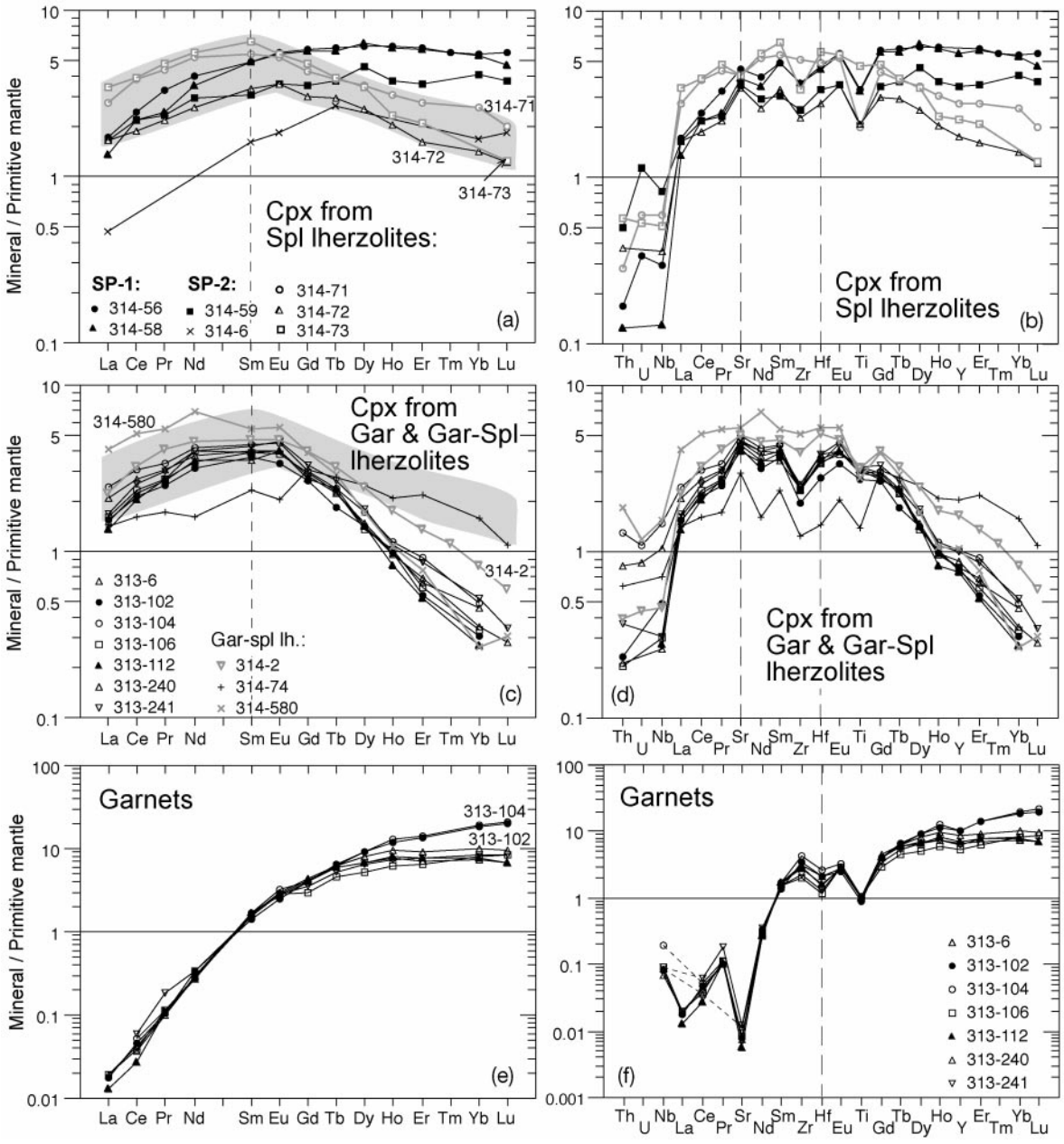

Fig. 5. Primitive mantle-normalized (Hofmann, 1988) trace element abundance patterns for garnets and clinopyroxenes: REE (left) and multi-element (right). Clinopyroxene patterns are shown separately for spinel peridotites (a and b) and for garnet-bearing peridotites (c and d). Low HREE and convex-upward REE patterns in clinopyroxene from some garnet-free peridotites (314-71, 314-72, 314-73) should be noted. Their REE patterns are outlined by grey shading in (a) and compared with patterns of clinopyroxene coexisting with garnet in (c). Cpx 314-6 is plotted using INAA analyses (Ionov *et al.*, 1993). Cpx patterns that seem to have a metasomatic LREE component are shown as grey lines and symbols.

This may also be the case for the HREE-rich garnet in xenolith 313-104 (Fig. 5e).

Minor HREE zoning was detected in clinopyroxene from both xenoliths (Fig. 7). In each sample, the clinopyroxene rims have higher HREE than the core. The HREE zoning may be related to major element zoning in the clinopyroxene (higher Al and lower Ca in the rims), apparently in response to a rise in temperature. Alternatively, higher HREE in clinopyroxene rims may be linked to replacement of garnet by HREE-poor kelyphite along rims and cracks and migration of HREE to nearby clinopyroxene.

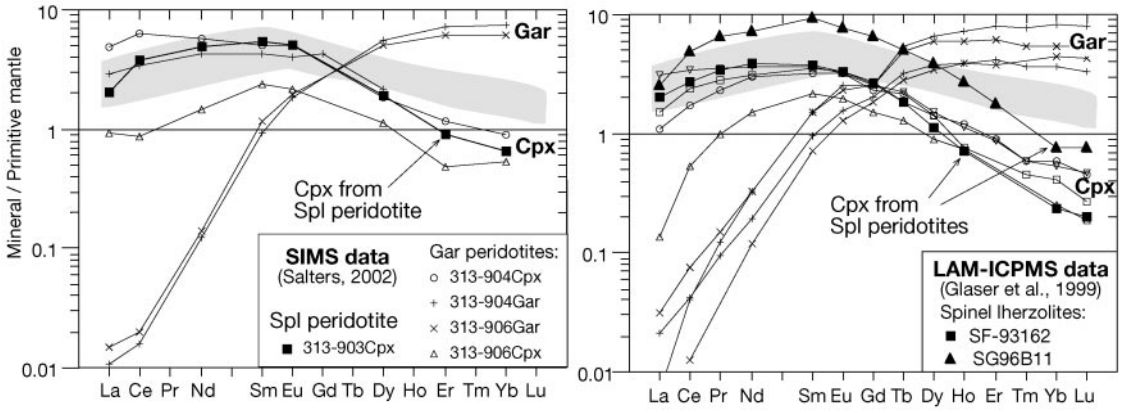

Fig. 6. Primitive mantle-normalized (Hofmann, 1988) REE patterns for garnet and clinopyroxene from Vitim peridotite xenoliths from other studies: (a) unpublished SIMS data of V. Salters (personal communication, 2002); (b) LA–ICP-MS data from Glaser *et al.* (1999). It should be noted that clinopyroxenes from spinel peridotites (filled symbols) are markedly depleted in HREE relative to MREE. Grey area outlines the field of HREE-depleted clinopyroxenes in spinel peridotites from this study (Fig. 5a).

Trace elements in bulk rocks

Primitive mantle-normalized trace element patterns for bulk rocks (solution ICP-MS data, Table 6) and minerals in two representative samples are shown in Fig. 8. Element abundances calculated for whole-rock samples from mineral analyses and modal compositions are nearly identical to those measured for HREE and MREE (from Lu to Sm), Sc, Y, Ti, Zr and Hf. By comparison, the abundances of less compatible elements (LREE, Sr, Nb, Ta, Th, U, Rb, Ba) in calculated bulk compositions are much lower than in whole-rock analyses. The differences do not appear to be related to rock type or modal composition. The clinopyroxenes (Fig. 5) show no evidence for metasomatic enrichment in highly incompatible elements relative to MREE. Furthermore, no accessory minerals of mantle origin that could host the highly incompatible elements have been observed in the rocks.

Mass balance problems for incompatible elements in mantle rocks have been earlier demonstrated for peridotites from many localities (Zindler & Jagoutz, 1986; Ionov *et al.*, 1995; Takazawa *et al.*, 2003), including Vitim (Ionov *et al.*, 1993; from INAA data). Enrichments in incompatible elements may be hosted in fluid inclusions or interstitial material of mantle origin (Eggins *et al.*, 1998; Bedini & Bodinier, 1999; Garrido *et al.*, 2000). Alternatively, these enrichments may reflect the combined effects of alteration and the presence of small amounts of host volcanic rock (Zindler & Jagoutz, 1986), which is common for xenoliths in kimberlites (Boyd *et al.*, 1997; Schmidberger & Francis, 2001; Pearson *et al.*, 2003). Host volcanic material is locally present at grain boundaries in some Vitim xenoliths (Fig. 2a and h). However, contamination of the Vitim xenoliths by the host magma cannot be the major reason for the excess whole-rock incompatible element abundances because some element ratios (Sr/Nd, Nb/La, Ba/Th) in many xenoliths are very different from those in the host volcanic rock (Fig. 9). Small degrees of post-eruption meteoric–hydrothermal alteration are common in the Vitim xenoliths (Fig. 2) and are likely to have affected the whole-rock trace element compositions. However, their effects in relation to those of hypothetical interstitial materials of mantle origin cannot be established unequivocally.

Because LREE levels in some whole-rock peridotites may have been increased during and after the eruption of their host, their MREE–HREE patterns are of most interest. The MREE–HREE abundances in SP-1 rocks are close to primitive mantle values (Fig. 10a). SP-2 samples 314-6 and 314-59 also have flat MREE–HREE patterns but at lower levels. The other four SP-2 xenoliths have continuously decreasing REE_N values from Sm to Lu in concert with the patterns of their clinopyroxenes (compare Figs 10a and 5a). The patterns of garnet-bearing peridotites can be grouped into three main types: (1) $MREE_N \sim HREE_N$; (2) $MREE_N > HREE_N$; (3) $MREE_N < HREE_N$. The first two types are similar to those identified in spinel peridotites. However, some Type-1 garnet lherzolites have much higher HREE contents than SP-1 lherzolites (up to 2 × primitive mantle in composite xenolith 313-4, Fig. 10b), and HREE abundances in Type-2 garnet-bearing rocks are higher than in SP-2 rocks with similar patterns (Fig. 10c and d). Type-3 patterns with fractionated $HREE_N > 1$ are unique to garnet peridotites. Importantly, the HREE-enriched pattern in the garnet peridotite part (113G) of composite xenolith 313-113 is complementary to the HREE-depleted patterns of the garnet–spinel (113SG) and spinel (113S) parts of that xenolith (Figs 2e–h and 10d).

Table 5: SIMS analyses of clinopyroxene and garnet in rim–core traverses

Sample:	313-54									313-102									
Mineral:	Garnet				Clinopyroxene					Clinopyroxene					Garnet				
	rim	at rim	core 1	core 2	rim	at rim	int	core 1	core 2	rim	at rim	int	core 1	core 2	rim	at rim	int	core 1	core 2
Sc	101·7	99·7	99·5	99·6	38·6	39·3	39·5	39·5	39·9	38·3	37·7	39·3	38·8	38·7	113	107	103	101	103
Ti	n.d.	n.d.	n.d.	n.d.	n.d.	n.d.	n.d.	n.d.	n.d.	2673	2692	2774	2792	2807	1035	995	973	990	1030
Sr	n.d.	n.d.	n.d.	n.d.	n.d.	n.d.	n.d.	n.d.	n.d.	58·0	58·7	63·2	62·0	61·3	0·20	0·21	0·25	0·18	0·22
Y	25·4	26·0	25·6	26·3	4·40	4·16	3·52	3·52	3·41	4·80	4·33	3·76	3·61	3·69	25·7	25·8	27·2	38·7	37·2
Zr	21·9	23·0	23·7	24·5	19·9	20·8	20·8	20·8	20·7	17·0	17·4	17·9	17·8	18·0	20·3	23·3	26·1	28·6	26·9
Nb	n.d.	n.d.	n.d.	n.d.	n.d.	n.d.	n.d.	n.d.	n.d.	0·46	0·43	0·43	0·43	0·44	0·058	0·059	0·049	0·066	0·073
Ba	0·004	0·007	0·007	0·004	0·135	0·866	0·028	0·028	0·035	n.d.	n.d.	n.d.	n.d.	n.d.				0·002	
La	0·005	0·005	0·006	0·006	1·50	1·95	1·42	1·42	1·46	0·87	0·88	0·92	0·89	0·88	0·004	0·010	0·004	0·005	0·008
Ce	0·045	0·043	0·050	0·051	4·48	5·19	4·32	4·32	4·28	2·98	2·98	3·09	3·04	3·06	0·055	0·045	0·048	0·055	0·058
Nd	0·32	0·34	0·33	0·35	4·49	4·49	4·40	4·40	4·21	3·48	3·30	3·48	3·52	3·51	0·35	0·35	0·29	0·33	0·34
Sm	0·52	0·51	0·51	0·54	1·51	1·55	1·48	1·48	1·44	1·34	1·23	1·36	1·29	1·36	0·48	0·47	0·46	0·48	0·49
Eu	0·31	0·32	0·34	0·34	0·54	0·55	0·55	0·55	0·53	0·48	0·48	0·48	0·46	0·48	0·34	0·29	0·30	0·33	0·33
Gd	1·77	1·91	1·89	1·91	1·63	1·69	1·53	1·53	1·59	0·20	0·19	0·19	0·19	0·18	1·72	1·73	1·80	1·99	2·05
Tb	0·45	0·46	0·44	0·47	0·22	0·22	0·20	0·20	0·21	1·45	1·44	1·53	1·42	1·46	0·42	0·46	0·45	0·54	0·52
Dy	3·59	3·60	3·71	3·83	1·09	1·07	0·95	0·95	0·90	1·08	1·04	0·98	0·98	0·88	3·46	3·74	4·09	5·10	5·03
Er	2·60	2·56	2·74	2·78	0·39	0·35	0·29	0·29	0·28	0·42	0·46	0·34	0·35	0·27	3·02	3·11	3·14	5·52	5·32
Yb	2·54	2·48	2·38	2·41	0·22	0·20	0·11	0·11	0·14	0·27	0·26	0·19	0·20	0·16	3·38	3·27	3·30	6·77	6·40
Lu	0·37	0·33	0·34	0·35	0·016	0·015	0·009	0·009	0·015	0·039	0·032	0·024	0·020	0·019	0·49	0·47	0·51	1·14	1·07
Hf	0·42	0·43	0·40	0·47	0·86	0·86	0·91	0·91	0·95	0·81	0·84	0·83	0·78	0·80	0·37	0·50	0·46	0·58	0·64

n.d., not determined; blank entry, below detection limit; int, intermediate (between core and rim).

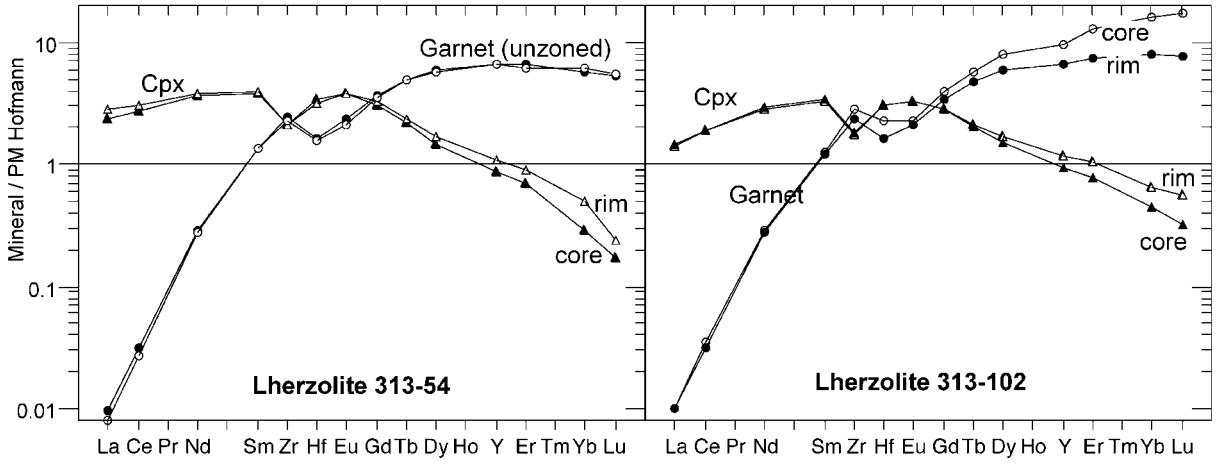

Fig. 7. Primitive mantle-normalized (Hofmann, 1988) trace element abundance patterns in cores and rims of clinopyroxene and garnet in two xenoliths determined by SIMS. Strong HREE core–rim zoning in garnet 313-102 and lack of zoning in garnet 313-54 should be noted.

DISCUSSION

Major and trace element relationships in the xenoliths

HREE abundances measured in several garnet-bearing peridotites (Types 1 and 3; Fig. 10b and d) are much higher than in primitive mantle estimates (Hofmann, 1988; Sun & McDonough, 1989). Lu abundances in these fertile (MgO $\leq$40%) Vitim xenoliths are also higher than in spinel peridotites from Mongolia and Horoman at similar MgO (Fig. 11b). On the other hand, several moderately depleted Vitim xenoliths (one garnet and several garnet–spinel and SP-2 peridotites with MgO >39·5%) plot below the Horoman MgO–Lu field in Fig. 11b. Overall, Fig. 11b shows that the MgO–Lu relationships are more complex in the Vitim xenoliths than for other mantle suites. Importantly, they are distinct from the MgO–Lu trend defined by the Horoman peridotites, which was shown to be consistent with an origin as residues of polybaric partial melting (Takazawa *et al.*, 2000).

Lu and Sc are positively correlated in the Vitim xenoliths (Fig. 12a). Many of the HREE-rich Vitim peridotites also have high abundances of Sc, an element that, like the HREE, strongly partitions into garnet (Table 4). The garnets have a broad range in Lu and Yb concentrations (Fig. 13), even in peridotites with similar MgO and Al_2O_3 contents (compare Figs 11b and 13). One should note, however, that at least some garnets rich in Lu and Yb are zoned and the high HREE may be present in their cores, but not the rims.

The abundances of elements with strong affinity for garnet in many Vitim xenoliths (Figs 11b and 12a) are inconsistent with the partial melting trend inferred for the Horoman peridotites (Takazawa *et al.*, 2000). By comparison, the abundances of moderately incompatible elements, such as Hf (Fig. 11c), Sm or Eu (not shown), which are mainly hosted by clinopyroxene, are similar to those in spinel lherzolites from Tariat and Horoman at a given per cent MgO. In particular, most of the Vitim xenoliths with anomalously high Lu and Yb (shown as grey-filled symbols in Fig. 11b and c) have Hf, Sm and Eu abundances below primitive mantle estimates and plot within the field of the Tariat xenoliths. It should be noted that Hf abundances in several SP-2 and garnet–spinel peridotites that plot above that field have been increased by metasomatism, together with their LREE abundances. Clinopyroxene in those samples (grey symbols in Fig. 5) is also enriched in Hf, Sm and LREE relative to clinopyroxene from the other xenoliths.

Overall, it appears that Lu and Hf are decoupled in the Vitim peridotites, relative to primitive mantle estimates, and to the partial melting-related trends defined by the Horoman and Tariat suites. The decoupling is most evident in some SP-2 and garnet–spinel peridotites (Lu too low) and in some garnet peridotites (Lu too high) (Fig. 12b). As a result, the Lu/Hf ratios in those rocks are not consistent with partial melting indices, such as MgO content (Fig. 14).

HREE–MREE fractionation during partial melting

The partial melting model of Takazawa *et al.* (2000) was used here to calculate the compositions of incremental (1% step) non-modal partial melting residues. For simplicity, no residual porosity (i.e. no trapped melt) was assumed because earlier studies have demonstrated that it significantly affects the results for HREE and MREE only at high melting degrees (>15%)

Table 6: Solution ICPMS analyses of whole-rock peridotites and their host volcanic rock

Rock:	Garnet lherzolites													Gar–Spl lherzolites			Spinel lherzolites						Ref. sa. JP-1		Host rock
Sample:	313-1	313-2	313-3	313-4	313-6	313-8	313-102	313-104	313-106	313-112	313-240	313-241	113G	113SG	313-37	314-2	113S	314-5	314-6	314-71	314-72	314-73	Niigata		87-1
Lab:	Mntp	Mntp	Gren	Gren	Gren	Gren	Gren	Niig	Niig	Gren	Mntp	Niig	Gren	Gren	Gren	Niig	Gren	Gren	Mntp	Niig	Niig	Gren	av. 2	R.V.	Mntp
Sc	20·5	11·5				19·9	19·3	17·3	14·9		15·6	17·4	29·3	11·9	10·6	15·2	4·3		9·0	9·0	12·2	7·3	7·5	7·2	15·8
Ti			926	1239	844	978	882	932	792	870		797	652	827	694	1257	539	398		903	641	1329	16·0		
V			86	127	109	103	100	88	75	105		77	79	99	104	71	58	71		54	61	98	18·2	27·6	
Co			91	88	91	82	88	107	111	85		109	96	96	87	109	97	109		121	114	94	113	116	
Rb	0·59	0·48	0·30	0·36	0·29	0·41	0·16	0·31	0·37	0·26	0·21	0·06	1·01	0·90	0·19	0·21	0·67	0·16	1·27	0·61	0·49	0·35	0·32	0·34	13·4
Sr	23·6	19·1	24·5	46·7	24·9	57·6	21·1	24·6	40·5	13·5	18·8	15·2	22	30·4	18	38·8	13·6	22·5	16·1	13·4	20·0	26·7	1·45	0·57	722
Y			3·82	7·51	3·42	5·71	5·23	4·15	3·64	4·38		4·08	8·48	2·83	2·86	4·21	0·68	0·51		1·25	1·50	1·96	0·107	0·10	
Zr	8·45	5·29	8·28	13·1	8·22	10·9	8·74	10·2	10·1	8·17	6·49	8·15	10·6	9·49	5·97	14·7	3·70	3·66	1·95	8·13	7·76	7·78	5·48	5·34	246
Nb	1·17	1·53	1·24	1·17	0·99	1·34	0·80	1·28	1·21	0·83	0·65	0·49	1·27	1·43	0·73	1·89	0·59	0·94	0·68	1·34	1·47	0·96	0·044	0·036	59·6
Cs			0·001	0·002	0·0015	0·002	0·001	0·003	0·005	0·004		0·001	0·003	0·003	0·002	0·003	0·002	0·001		0·006	0·007	0·001	0·039	0·035	
Ba	6·9	11·4	46·6	26·2	16·5	27·6	8·4	14·7	9·1	3·7	19·4	3·2	22·4	23·5	10·0	75·6	10·4	5·9	19·2	10·5	10·5	52·7	10·0	9·8	368
La	0·95	1·48	1·22	1·08	0·82	1·41	0·56	0·80	1·07	0·37	0·77	0·34	0·98	1·09	0·65	2·05	0·31	0·81	0·62	0·62	1·00	0·97	0·028	0·030	25·8
Ce	1·80	1·91	1·72	1·84	1·31	2·05	1·12	1·90	2·00	1·06	1·13	0·89	1·50	2·12	1·25	2·40	0·66	1·10	0·71	1·42	1·91	1·58	0·062	0·054	60·3
Pr	0·30	0·29	0·29	0·33	0·23	0·36	0·19	0·28	0·29	0·15	0·19	0·15	0·22	0·30	0·20	0·44	0·10	0·16	0·15	0·18	0·25	0·26	0·008	0·007	7·86
Nd	1·39	1·28	1·35	1·62		1·58	0·95	1·32	1·36	0·81	0·94	0·82	0·95	1·40	0·96	1·98	0·50	0·66	0·64	0·86	1·07	1·3	0·031	0·033	35
Sm	0·42	0·33	0·39	0·53	0·33	0·48	0·31	0·43	0·40	0·27	0·31	0·31	0·30	0·37	0·26	0·52	0·15	0·13	0·15	0·23	0·28	0·35	0·009	0·013	7·5
Eu	0·16	0·12	0·14	0·21	0·13	0·17	0·13	0·15	0·14	0·12	0·12	0·12	0·13	0·14	0·11	0·19	0·05	0·043	0·05	0·08	0·095	0·13	0·003	0·003	2·42
Gd	0·59	0·41	0·51	0·81	0·46	0·66	0·48	0·57	0·52	0·45	0·47	0·46	0·56	0·45	0·37	0·64	0·16	0·12	0·17	0·26	0·30	0·42	0·011	0·013	6·97
Tb	0·10	0·064	0·090	0·165	0·088	0·12	0·098	0·10	0·087	0·092	0·086	0·088	0·13	0·072	0·065	0·10	0·022	0·018	0·025	0·039	0·047	0·064	0·003	0·003	0·93
Dy	0·73	0·40	0·60	1·20	0·55	0·85	0·71	0·62	0·55	0·64	0·60	0·60	1·08	0·44	0·44	0·66	0·11	0·088	0·16	0·22	0·27	0·36	0·014	0·018	4·88
Ho	0·17	0·082	0·13	0·27	0·12	0·20	0·18	0·13	0·12	0·16	0·14	0·14	0·29	0·086	0·102	0·14	0·019	0·014	0·036	0·041	0·052	0·067	0·004	0·004	0·78
Er	0·50	0·22	0·41	0·82	0·36	0·60	0·57	0·39	0·35	0·48	0·42	0·41	0·95	0·25	0·30	0·38	0·05	0·032	0·10	0·11	0·14	0·17	0·013	0·014	1·73
Tm	0·078	0·032									0·064								0·015						0·20
Yb	0·49	0·19	0·36	0·75	0·31	0·60	0·62	0·37	0·31	0·50	0·42	0·39	1·042	0·192	0·308	0·35	0·03	0·018	0·10	0·09	0·12	0·111	0·019	0·021	1·16
Lu	0·083	0·031	0·057	0·120	0·050	0·093	0·103	0·057	0·047	0·078	0·071	0·061	0·167	0·029	0·051	0·053	0·007	0·003	0·018	0·013	0·017	0·015	0·004	0·005	0·169
Hf	0·245	0·167	0·212	0·318	0·204	0·282	0·200	0·259	0·249	0·211	0·183	0·211	0·175	0·239	0·171	0·376	0·102	0·079	0·053	0·221	0·176	0·257	0·118	0·120	5·94
Ta		0·078	0·147	0·151	0·083	0·189	0·030	0·054	0·056	0·035	0·030	0·016	0·060	0·077	0·098	0·096	0·028	0·081		0·062	0·072	0·050	0·005	0·004	3·46
Pb	0·16	0·11	0·12	0·11	0·09	0·15	0·12	0·16	0·103	0·17	0·056	0·10	0·67	0·19	0·10	0·12	0·12	0·52	0·33	0·049	0·11	0·10	0·10	0·09	4·18
Th	0·091	0·108	0·066	0·070	0·059	0·094	0·037	0·093	0·096	0·046	0·038	0·029	0·087	0·108	0·057	0·114	0·036	0·056	0·036	0·077	0·114	0·056	0·013	0·012	3·73
U	0·023	0·032	0·028	0·023	0·02	0·029	0·013	0·032	0·039	0·021	0·021	0·013	0·026	0·020	0·014	0·048	0·008	0·017	0·011	0·017	0·031	0·021	0·012	0·012	0·45

Analytical laboratories: Mntp, Montpellier; Niig, Niigata; Gren, Grenoble. Recommended values (R.V.) for JP-1 are from Makishima & Nakamura (1997). Blank entries, not determined.

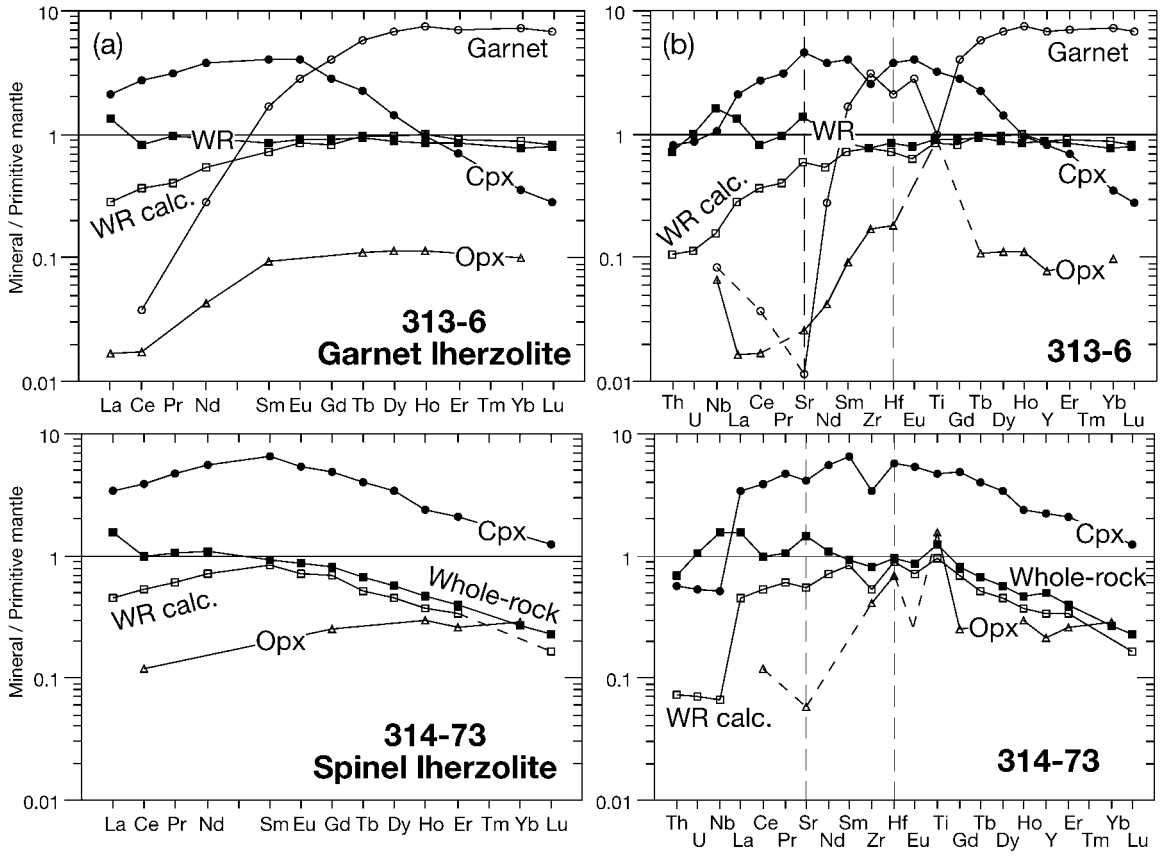

Fig. 8. Primitive mantle-normalized (Hofmann, 1988) trace element abundance patterns for whole rocks (WR) and minerals in garnet lherzolite 313-6 and spinel lherzolite 314-73: (a) REE; (b) multi-element. Open squares show whole-rock compositions calculated from mineral analyses and modal abundances.

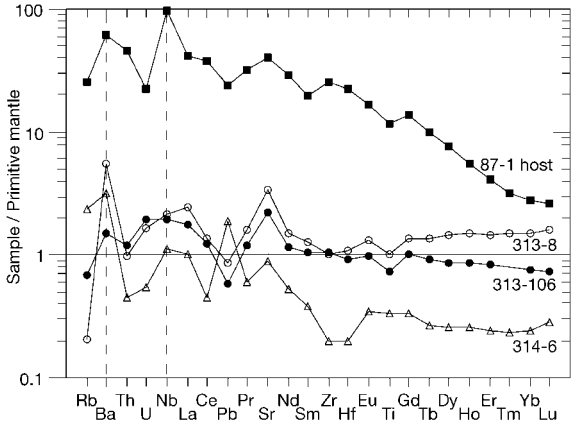

Fig. 9. Primitive mantle-normalized (Hofmann, 1988) trace element abundance patterns for selected whole-rock xenoliths in comparison with the host volcanic rock. Differences in pattern shapes and some element ratios argue against a major role of contamination by the host in the incompatible element enrichment of the xenoliths.

(Takazawa *et al*., 2000; Hellebrand *et al*., 2002). The initial trace element abundances are those for primitive mantle after Hofmann (1988). Three starting modal compositions were used to cover a broad range of modal garnet and clinopyroxene in the source (wt %): (1) Cpx, 18·5 (garnet-free); (2) Gar, 3; Cpx, 25; (3) Gar, 9; Cpx, 13. Cpx/melt partition coefficients ($D^{cpx/l}$) for source (1) are after Hart & Dunn (1993). $D^{cpx/l}$ and $D^{gar/l}$ for sources (2) and (3) are after Johnson (1998). The use of much higher $D^{cpx/l}$ values after Blundy *et al*. (1998) (applicable only at incipient melting) yields somewhat higher REE contents in the residues but does not affect MREE/HREE ratios (Hellebrand *et al*., 2002).

The *P*–*T* data for the Vitim xenoliths in combination with experimental results on peridotite phase boundaries (Fig. 4) indicate that a rise in temperature by 100–200°C would drive most of the garnet peridotites to the spinel stability field (probably before the beginning of dry partial melting). This is consistent with widespread replacement of garnet with opx–spl aggregates in sample 314-2 (Fig. 2d) and some other Vitim xenoliths. It follows that partial melting of a presumed fertile protolith for the Vitim peridotite series probably took place in the spinel peridotite field, represented by modal source composition (1) above. Modal source composition (2) implies that partial

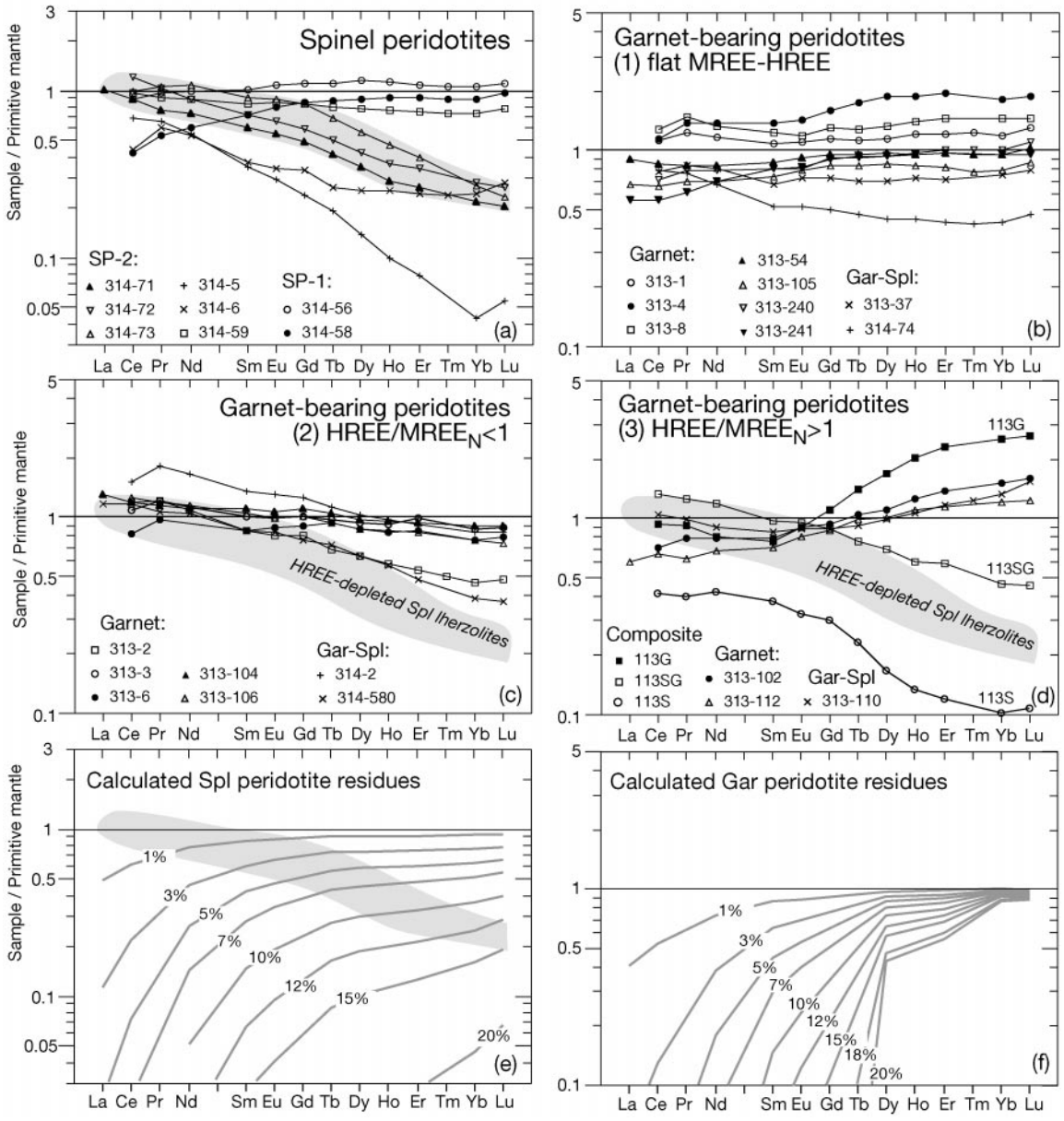

Fig. 10. (a–d) Primitive mantle-normalized (Hofmann, 1988) REE abundance patterns for whole-rock xenoliths. Garnet-bearing peridotites are grouped by REE patterns: (1) $MREE_N \sim HREE_N$, (2) $MREE_N > HREE_N$, (3) $MREE_N < HREE_N$. Grey area in (a) outlines the field of SP-2 peridotites with high MREE/HREE; it is also shown for comparison in (c) and (d). La is not plotted for rocks in which high La/Ce ratios appear to be a result of alteration (see Fig. 8). (e) and (f) show compositions of incremental (1% step) non-modal partial melting residues (no residual porosity) calculated using the model of Takazawa *et al.* (2000). The initial REE abundances are those in the primitive mantle after Hofmann (1988). Initial modal compositions (wt %): (e) Spl, 2·5; Cpx, 18·5; Opx, 28; Ol, 51; (f) Gar, 9; Cpx, 13; Opx, 21; Ol, 57. Whole-rock REE patterns in many Vitim xenoliths cannot be produced by partial melting in either the garnet or the spinel facies.

melting begins in the garnet stability field at low modal garnet (3%) and continues in the spinel stability field after the garnet is exhausted. High modal Cpx in source (2) reflects low CaO in Cpx equilibrated with melt and garnet at high P–T (e.g. Johnson, 1998) as discussed by Takazawa *et al.* (2000). Source (3) has too much garnet to be relevant to likely partial melting conditions inferred from pressure estimates for the Vitim peridotites and was used to illustrate an extreme case of garnet-controlled REE fractionation.

REE patterns in melting residues for modal source compositions (1) and (3) are shown in Fig. 10e and f. The patterns of fertile spinel and garnet peridotites with $MREE/HREE_N \sim 1$ (Fig. 10a and b) are consistent with low (1–4%) degrees of melting in the spinel field. Several less fertile peridotites (314-6, 314-74) can

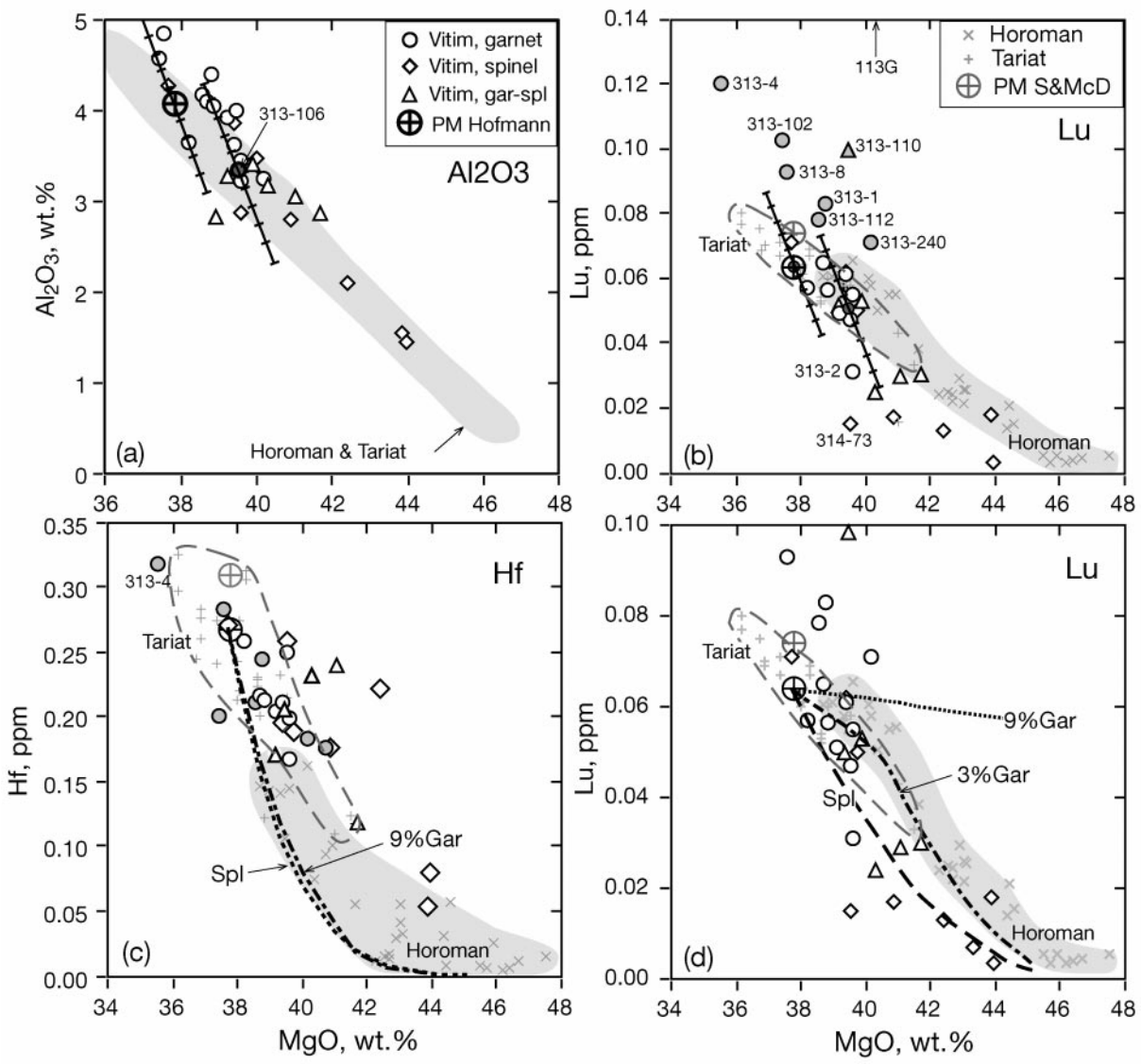

Fig. 11. Co-variation diagrams for Al_2O_3 (a), Lu (b, d) and Hf (c) vs MgO for whole-rock peridotites. Symbols, other data and data sources are as in Fig. 3. Circles with a cross show primitive mantle (PM) compositions after Hofmann (1988) (black) and Sun & McDonough (1989) (grey). Grey dashed line contours Tariat xenoliths; grey fields outline combined Tariat–Horoman series in (a) and Horoman field in (b–d). Grey-filled symbols for Vitim garnet-bearing peridotites in (b) and (c) are 'anomalous' samples that plot above the Tariat–Horoman MgO–Al_2O_3 field (grey) in (a). Black straight lines with ticks in (a) and (b) show calculated results of addition or removal of 0·5–5% of garnet from two initial compositions: primitive mantle and moderately depleted peridotite 313-106. Black dashed lines in (c) and (d) are calculated compositions of residues after incremental non-modal partial melting of primitive mantle (Hofmann, 1988) using the algorithm and parameters from Takazawa *et al.* (2000). Three sets of initial modal compositions were used for the primitive mantle (wt %): (1) Spl, 2·5; Cpx, 18·5; Opx, 28; Ol, 51; (2) Gar, 3; Cpx, 25; Opx, 18; Ol, 54; (3) Gar, 9; Cpx, 13; Opx, 21; Ol, 57.

be produced by 5–12% of melting followed by minor LREE–MREE enrichment by metasomatism. $D^{gar/l}$ for Yb and Lu are very high (6·6 and 7·1, respectively) and result in bulk partition coefficients close to unity for the garnet-rich source (3). For that reason, melting in the garnet field has little effect on Lu and Yb in the residues and cannot explain their broad range in the Vitim peridotites (Fig. 10f). By comparison, residual garnet peridotites have $HREE/MREE_N > 1$ and strongly fractionated MREE (e.g. high Dy/Gd). Only four Vitim garnet peridotites have similar patterns (Fig. 10d), but all of them have much higher HREE abundances than primitive mantle. Finally, the HREE-depleted compositions (Fig. 10a, c and d) cannot be produced by partial melting in either the spinel or the garnet stability field.

I conclude that the REE distribution in many whole-rock Vitim peridotites, which was previously

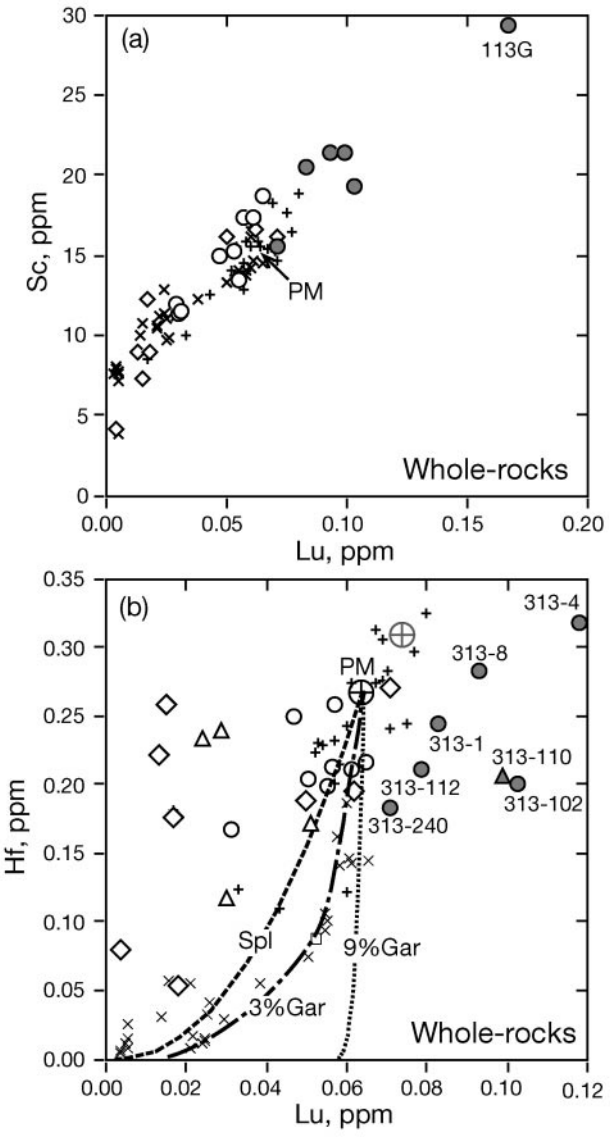

Fig. 12. A plot of Lu vs Sc (a) and Hf (b) in whole-rock Vitim peridotites. Symbols, other data, partial melting trends and data sources are as in Fig. 11.

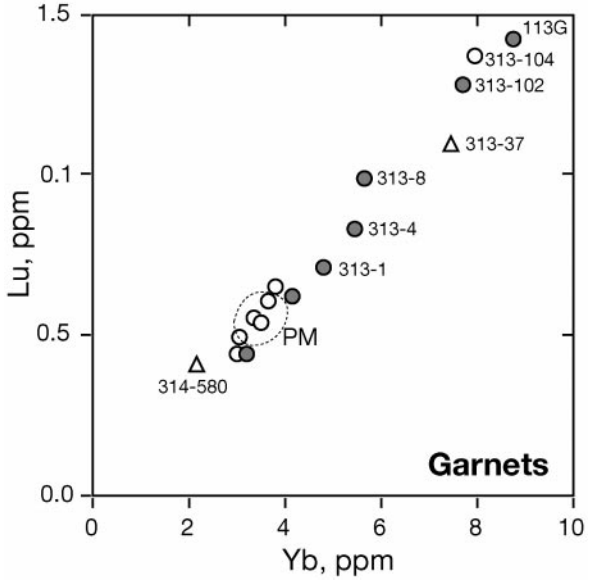

Fig. 13. A plot of Lu vs Yb in Vitim garnets [this study and Ionov *et al.* (1993)]. Symbols are as in Fig. 11. Dashed line contours garnet compositions calculated for a lherzolite with primitive mantle (Hofmann, 1988) Lu and Yb whole-rock abundances containing 12% of garnet and 12% clinopyroxene (using gar/cpx ratios of 25 for Lu and 20 for Yb calculated from averaged data in Table 4).

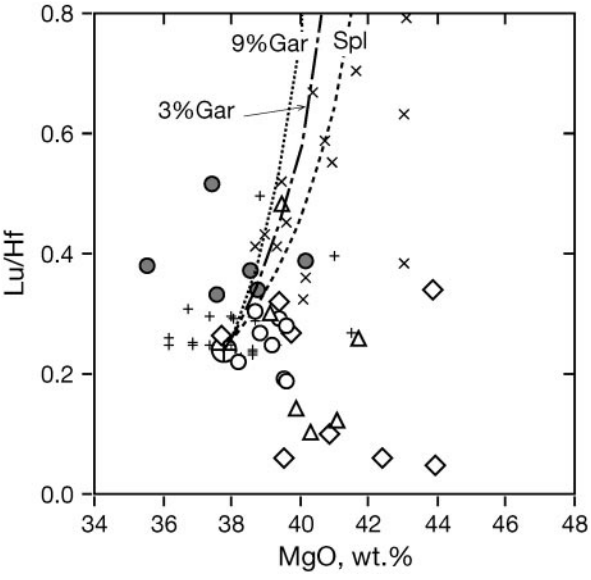

Fig. 14. A plot of Lu/Hf vs MgO in whole-rock Vitim peridotites. Symbols, other data and data sources are as in Fig. 11. Lu/Hf ratios for Horoman peridotites with MgO ≥44% have not been plotted because Hf abundances in those highly depleted rocks have been affected by metasomatism (Takazawa *et al.*, 2000, fig. 7).

characterized as anomalous based on qualitative arguments, is inconsistent with the REE patterns of melting residues of a single fertile peridotite source in either the garnet or the spinel stability field. Some of those patterns could probably be explained by complex processes involving local impregnation of the protolith with variable amounts of HREE-rich or HREE-poor melts before or after partial melting, but such *ad hoc* scenarios are not likely and require distinct events to explain each kind of REE pattern. Kempton *et al.* (1999*a*) suggested that HREE-depleted clinopyroxenes in some spinel peridotites from Pali-Aike could be produced in a complex event involving enrichment of refractory melting residues by liquids generated from fertile garnet peridotites. However, such a model is much less likely to explain HREE depletions in Cpx-rich and garnet-bearing peridotites (Fig. 10a and c).

Furthermore, mainly depleted Sr–Nd isotope compositions found in the fertile Vitim peridotites (Ionov & Jagoutz, 1989) argue against widespread melt metasomatism in those rocks.

The calculated trace element compositions for the melting residues are also plotted in Fig. 11c and d vs MgO [estimated following the approach of Takazawa *et al.* (2000)]. These results further demonstrate an earlier inference of Takazawa *et al.* (2000) that Lu distribution in the Horoman peridotites is consistent with polybaric partial melting at low initial modal garnet. They also show that MgO–Lu relationships in many 'normal' Vitim peridotites can be explained by partial melting of a source either with spinel peridotite mineralogy or with low initial garnet contents, as for the Horoman series (Fig. 11d). By contrast, the 'anomalous' (Lu-rich and Lu-poor) Vitim xenoliths cannot be produced by partial melting of a primitive source either in garnet or spinel facies mantle. Partial melting of a garnet-rich source (3) is obviously inconsistent with the MgO–Lu peridotite trend (Fig. 11d). These inferences are even more apparent from the data and model calculations on the Lu–Hf plot (Fig. 12b).

Chemical compositions and heterogeneous garnet distribution

Several chemical characteristics of the Vitim peridotites cannot be a result of partial melting alone and must have been produced or significantly affected by a different process. These include Mg–Ca–Al variations in whole rocks, HREE depletion in spinel and garnet peridotites, variable HREE enrichment in garnet peridotites, and HREE variations in clinopyroxenes and garnets. The least affected partial melting indicator appears to be the MgO content in the bulk rocks.

This section will examine a hypothesis that the unusually broad scatter shown by many Vitim peridotites on major element co-variation plots (Fig. 3) reflects heterogeneous distribution of minerals, mainly garnet, on a scale close to or exceeding the size of the largest xenoliths we studied. Such a possibility is strongly indicated by modal variations on a centimetre scale found in several composite garnet-bearing Vitim xenoliths, such as vaguely defined spinel, garnet–spinel and garnet lherzolite domains in xenolith 313-113 (Table 1; Fig. 2e–h) or a garnet-rich zone in xenolith 313-4 (Fig. 2c). Another possibility is a vague gradational layering in the mantle, like that observed in some peridotite massifs (e.g. Garrido & Bodinier, 1999; Lenoir *et al.*, 2001). Importantly, such heterogeneities must be formed, or at least enhanced, after partial melting. Press *et al.* (1986) found that several spinel lherzolite xenoliths from Tariat have anomalous contents of Ca, Al and Ti as well deviating from the general correlations between whole-rock MgO or olivine Mg-numbers [$Mg/(Mg + Fe)_{at}$]. Because all these parameters are expected to vary consistently in partial melting residues, Press *et al.* (1986) envisaged 'mechanical segregation' of clinopyroxene as a result of 'metamorphic differentiation' following partial melting to explain the major element compositions of those 'anomalous' xenoliths. Wallace & Green (1991) argued that metamorphic differentiation may take place in a crystallizing mantle diapir because of preferential amphibole precipitation from migrating alkali-rich melts in the most fertile residual peridotites.

I speculate that a heterogeneous peridotite series initially derived by different degrees of partial melting and located in the depth range overlapping the transition between the garnet and the spinel lherzolite facies in the lithospheric mantle could undergo near-solidus 'metamorphic' differentiation on a centimetre–metre scale. After a partial melting event, these rocks may initially be spinel peridotites if garnet is not stable in that depth range at high temperatures. Garnet stability, in addition to the P–T conditions, is strongly dependent on the whole-rock Al abundances and Cr/(Cr + Al) values (Nickel, 1986; Webb & Wood, 1986; Robinson & Wood, 1998; Klemme & O'Neill, 2000). As the partial melting residues cool down, garnet first becomes stable and starts to form in rocks with the highest Al and lowest Cr/(Cr + Al) at a given T. This must be the case regardless of whether the cooling takes place at constant pressure (in the lithospheric mantle) or in a rising asthenospheric diapir (in which case the cooling is accompanied by a pressure decrease). The early formation of garnet in the most fertile domains of the peridotite series may result in local migration of garnet components (mainly Al) to the site of initial garnet crystallization from adjacent less fertile domains. In the case of slow cooling, this process may produce small-scale modal and chemical heterogeneity if the rate of the metamorphic migration is high enough. Such a process will be strongly assisted by the presence of small amounts of a melt because grain diffusion is slow. This general concept has some similarities to the 'auto-metasomatism' model outlined by Kempton *et al.* (1999*b*) for Pali-Aike peridotites in the sense that REE fractionation is produced by chemical fractionation within a heterogeneous peridotite series following the major partial melting event.

A relatively simple way to assess the effects of 'metamorphic differentiation' is to consider it as a mechanical segregation of garnet, that is, addition or removal of certain amounts of garnet from a peridotite. I calculated major element compositions of hypothetical peridotites, with 0·5–5% of garnet either removed from or added to (1) a primitive peridotite (Hofmann,

1988) and (2) slightly depleted peridotite 313-106 (Fig. 11a). Garnet compositions used in the calculations were those of 313-54 for the primitive mantle and 313-106 for the peridotite 313-106. The garnets typically contain some 23% Al_2O_3, 5% CaO, 7·5% FeO and 21–22% MgO. It is apparent that garnet removal or addition strongly affects Al_2O_3 (Fig. 11a), but has smaller effects on other major oxides. Garnet addition may explain the Al-enriched rocks on the MgO–Al_2O_3 plot, but the complementary Al-depleted peridotites should probably be more abundant (Fig. 11a). Their scarcity might be related to preferential sampling of garnet-rich xenoliths in the field. Fractionation of $\leq$5% of garnet from fertile peridotites may also explain the broad range of Al_2O_3 at a given CaO content in the Vitim peridotites (Fig. 3a; modelling results not shown).

Model calculations analogous to those presented in the previous section for major elements were also performed for trace elements. They show (Fig. 11b) that addition of $\leq$5% of garnet (with an average Lu content) from primitive or moderately depleted peridotites is not sufficient to yield high Lu in many Vitim garnet peridotites. Similarly, removal of $\leq$5% of garnet from hypothetical garnet-bearing sources is not sufficient to produce low Lu in some Vitim spinel peridotites. Furthermore, large Lu and Yb variations in garnets (by a factor of four; Fig. 13) indicate that garnet/melt (or garnet/cpx) REE fractionation is an important factor (in addition to garnet redistribution) in determining the HREE budgets in the Vitim peridotites because of very high $D^{gar/l}$ for those elements.

Effects of local garnet-controlled trace element fractionation

It appears from the discussion in the previous two sections that neither partial melting nor hypothetical metamorphic garnet segregation can explain the REE–Hf relationships in the Vitim peridotite series. It is likely, therefore, that local garnet-controlled REE fractionation following the major partial melting event may be an important factor in determining the HREE budgets in many Vitim peridotites. This may be possible if some garnet peridotites had some degree of chemical exchange with garnet-free (or garnet-poor) domains on a scale beyond that of the largest xenoliths in this study ($\sim$20 cm). In such a case, early garnet nucleation in the most fertile peridotites on cooling would result in migration and redistribution of elements with high garnet/cpx (or garnet/melt) ratios between more and less fertile domains. HREE zoning in garnet 313-102 may be consistent with such a process as well. Its HREE-rich cores may have been produced at an early stage of this process (with corresponding HREE depletion in adjacent spinel peridotite) whereas the rim compositions may correspond to later sub-solidus REE redistribution on a smaller scale.

Petrographic evidence of different modal contents and textural relationships of garnet and spinel in composite xenolith 313-113 (Figs. 2e–h) may provide a physical representation of such a process. The HREE–MREE patterns in the three zones of this xenolith cannot result from different degrees of partial melting (Fig. 10d–f). Instead, they appear to indicate a significant chemical exchange (and possibly, trace element equilibration) on a centimetre scale between adjacent domains of residual peridotite because the high HREE/MREE values in the garnet-rich zone (113G) are complementary to the low HREE/MREE in the garnet-poor (113SG) and garnet-free (113S) parts of the xenolith (Fig. 10d). Lu and Yb abundances in garnet 113G [INAA data from Ionov *et al.* (1993)] are the highest observed in the Vitim xenoliths (Fig. 13) and are a major factor (in addition to high modal garnet) in the strong whole-rock enrichment of 113G in HREE.

The presence of interstitial melt (for example, as a result of the residual porosity of partial melting residues) may be an important factor in the late-stage redistribution of HREE. The interstitial and poikilitic clinopyroxene in garnet peridotites (Fig. 2b) may have formed from such melts. As discussed above, clinopyroxenes in a few spinel and garnet–spinel Vitim peridotites have higher LREE, Sm and Eu abundances than in the other peridotites (Figs 5a and 6). These appear to be too high for partial melting residues and may result from interaction with evolved fractionation products of such initial interstitial melts.

Inferences for the Lu–Hf isotopic system

The evidence on Lu–Hf decoupling in the Vitim peridotites may be relevant to Lu–Hf isotopic systematics in garnet and garnet–spinel peridotites worldwide (regardless of whether the differentiation mechanisms proposed in this study are correct). The decoupling appears to take place in chemically heterogeneous peridotite mantle during the spinel-to-garnet peridotite phase transition on cooling, but could also occur as a result of pressure increase. Such phenomena may be common in the upper part of the garnet-facies mantle.

If the Lu migration and Lu–Hf decoupling take place shortly after the melting event (and assuming no later disturbance by metasomatism) whole-rock Lu–Hf isotope data may yield a nearly correct depletion age, but the relationships between the Hf-isotope, modal and chemical compositions of the peridotites may be disturbed (Figs 12b and 14). If the decoupling takes place much later, the depletion record in terms of HREE–MREE patterns will be obliterated as well as the evidence for the timing of depletion as recorded by

Lu–Hf isotopic systematics. The data for Vitim peridotites indicate that the Lu–Hf decoupling is mainly due to Lu redistribution driven by the very high garnet/melt and garnet/cpx partition coefficients for Lu. If Hf abundances and isotopic compositions are not re-equilibrated simultaneously, the Lu–Hf model or isochron age estimates in peridotite series affected by such processes may be biased or have no meaning.

ACKNOWLEDGEMENTS

This study has benefited from advice and support from I. Ashchepkov, N. Arndt, J.-L. Bodinier, C. Chauvel, V. Salters and D. Weis. Assistance by E. Takazawa with XRF and ICP-MS analyses at Niigata and modelling is greatly appreciated. Analytical assistance was provided by B. Boyer, F. Keller, C. Merlet, N. Pearson, S. Pourtales, A. Sharma and A. Zanetti. Reviews by P. Kempton, G. Pearson and V. Salters, and editorial comments by F. Frey have helped to improve the manuscript. Funding was provided by Centre National de la Recherche Scientifique (France), Université de Grenoble, Université Libre de Bruxelles and Australian Research Council.

REFERENCES

Ashchepkov, I. V. (1991). *Deep-seated Xenoliths of the Baikal Rift*. Novosibirsk: Nauka (in Russian).

Ashchepkov, I. V., Dobretsov, N. L. & Kalmanovich, M. A. (1989). Garnet peridotite xenoliths from alkalic picritoid and basanitoid of the Vitim Plateau. *Transactions (Doklady) USSR Academy of Sciences: Earth Science Section* **302**, 156–159.

Bedini, R. M. & Bodinier, J.-L. (1999). Distribution of incompatible trace elements between the constituents of spinel peridotite xenoliths: ICP-MS data from the East African rift. *Geochimica et Cosmochimica Acta* **63**, 3883–3900.

Blundy, J. D., Robinson, J. A. C. & Wood, B. J. (1998). Heavy REE are compatible in clinopyroxene on the spinel lherzolite solidus. *Earth and Planetary Science Letters* **160**, 493–504.

Bottazzi, P., Ottolini, L., Vannucci, R. & Zanetti, A. (1994). An accurate procedure for the quantification of rare earth elements in silicates. In: Benninghoven, A., Nihei, Y., Shimizu, R. & Werner, H. V. (eds) *Secondary Ion Mass Spectrometry, SIMS IX*. Chichester: John Wiley, pp. 927–930.

Boyd, F. R. (1989). Compositional distinction between oceanic and cratonic lithosphere. *Earth and Planetary Science Letters* **96**, 15–26.

Boyd, F. R., Pokhilenko, N. P., Pearson, D. G., Mertzman, S. A., Sobolev, N. V. & Finger, L. W. (1997). Composition of the Siberian cratonic mantle: evidence from Udachnaya peridotite xenoliths. *Contributions to Mineralogy and Petrology* **128**, 228–246.

Brey, G. P. & Köhler, T. (1990). Geothermobarometry in four-phase lherzolites II. New thermobarometers, and practical assessment of existing thermobarometers. *Journal of Petrology* **31**, 1353–1378.

Caroll-Webb, S. A. & Wood, B. J. (1986). Spinel–pyroxene–garnet relationships and their dependence on Cr/Al ratio. *Contributions to Mineralogy and Petrology* **92**, 471–480.

Eggins, S. M., Rudnick, R. L. & McDonough, W. F. (1998). The composition of peridotites and their minerals: a laser ablation ICP-MS study. *Earth and Planetary Science Letters* **154**, 53–71.

Esin, S. V., Ashchepkov, I. V. & Ponomarchuk, V. A. (1995). *Petrogenesis of Alkaline Basaltoids from the Vitim Plateau (Baikal Rift Zone)*. Novosibirsk: UIGGM SB RAS (in Russian).

Fujinawa, A. & Green, T. H. (1997). Partitioning behavior of Hf and Zr between amphibole, clinopyroxene, garnet and silicate melts at high pressure. *European Journal of Mineralogy* **9**, 379–391.

Garrido, C. & Bodinier, J.-L. (1999). Diversity of mafic rocks in the Ronda peridotite: evidence for pervasive melt/rock reaction during heating of subcontinental lithosphere by upwelling asthenosphere. *Journal of Petrology* **40**, 729–754.

Garrido, C. J., Bodinier, J.-L. & Alard, O. (2000). Incompatible trace element partitioning and residence in anhydrous spinel peridotites and websterites from the Ronda orogenic peridotite. *Earth and Planetary Science Letters* **181**, 341–358.

Glaser, S. M., Foley, S. F. & Günther, D. (1999). Trace element compositions of minerals in garnet and spinel peridotite xenoliths from the Vitim volcanic field, Transbaikalia, eastern Siberia. *Lithos* **48**, 263–285.

Halliday, A. N. (1999). Mantle geochemistry: unmixing Hawaiian cocktails. *Nature* **399**, 733–734.

Hart, S. R. & Dunn, T. (1993). Experimental cpx/melt partitioning of 24 trace elements. *Contributions to Mineralogy and Petrology* **113**, 1–8.

Hart, S. R. & Zindler, A. (1986). In search of a bulk-Earth composition. *Chemical Geology* **57**, 247–267.

Hellebrand, E., Snow, J. E., Hoppe, P. & Hofmann, A. W. (2002). Garnet-field melting and late-stage refertilization in 'residual' abyssal peridotites from the Central Indian Ridge. *Journal of Petrology* **43**, 2305–2338.

Hofmann, A. W. (1988). Chemical differentiation of the Earth: the relationship between mantle, continental crust, and oceanic crust. *Earth and Planetary Science Letters* **90**, 297–314.

Ionov, D. (2002). Mantle structure and rifting processes in the Baikal–Mongolia region: geophysical data and evidence from xenoliths in volcanic rocks. *Tectonophysics* **351**, 41–60.

Ionov, D. A. & Hofmann, A. W. (1995). Nb–Ta-rich mantle amphiboles and micas: implications for subduction-related metasomatic trace element fractionations. *Earth and Planetary Science Letters* **131**, 341–356.

Ionov, D. A. & Jagoutz, E. (1989). Sr and Nd isotopic composition in minerals of garnet and spinel peridotite xenoliths from the Vitim Highland: first data for mantle inclusions from the USSR. *Transactions (Doklady) USSR Academy of Sciences: Earth Science Section* **301**, 232–236.

Ionov, D. A., Savoyant, L. & Dupuy, C. (1992). Application of the ICP-MS technique to trace element analysis of peridotites and their minerals. *Geostandards Newsletter* **16**, 311–315.

Ionov, D. A., Ashchepkov, I. V., Stosch, H.-G., Witt-Eickschen, G. & Seck, H. A. (1993). Garnet peridotite xenoliths from the Vitim volcanic field, Baikal region: the nature of the garnet–spinel peridotite transition zone in the continental mantle. *Journal of Petrology* **34**, 1141–1175.

Ionov, D. A., Prikhod'ko, V. S. & O'Reilly, S. Y. (1995). Peridotite xenoliths from the Sikhote-Alin, south-eastern Siberia, Russia: trace element signatures of mantle beneath a convergent continental margin. *Chemical Geology* **120**, 275–294.

Ionov, D. A., O'Reilly, S. Y. & Griffin, W. L. (1998). A geotherm and lithospheric cross-section for central Mongolia. In: Flower, M. J. F., Chung, S.-L., Lo, C.-H. & Lee, T. Y. (eds) *Mantle Dynamics and Plate Interactions in East Asia. American Geophysical Union, Geodynamics Series* **27**, 127–153.

Johnson, K. T. M. (1998). Experimental determination of partition coefficients for rare earth and high-field-strength elements between clinopyroxene, garnet, and basaltic melt at high pressures. *Contributions to Mineralogy and Petrology* **133**, 60–68.

Kempton, P. D., Hawkesworth, C. J., Lopez-Escobar, L., Pearson, D. G. & Ware, A. J. (1999*a*). Spinel ± garnet lherzolite xenoliths from Pali Aike, Part 2: Trace element and isotopic evidence on the evolution of lithospheric mantle beneath southern Patagonia. In: Gurney, J. J., Gurney, J. L., Pascoe, M. D. & Richardson, S. H. (eds) *Proceedings of the 7th International Kimberlite Conference*. Cape Town: Red Roof Design, pp. 415–428.

Kempton, P. D., Lopez-Escobar, L., Hawkesworth, C. J., Pearson, D. G., Wright, D. W. & Ware, A. J. (1999*b*). Spinel ± garnet lherzolite xenoliths from Pali Aike, Part 1: petrography, mineral chemistry and geothermobarometry. In: Gurney, J. J., Gurney, J. L., Pascoe, M. D. & Richardson, S. H. (eds) *Proceedings of the 7th International Kimberlite Conference*. Cape Town: Red Roof Design, pp. 403–414.

Kern, H., Burlini, L. & Ashchepkov, I. V. (1996). Fabric-related seismic anisotropy in upper-mantle xenoliths: evidence from measurements and calculations. *Physics of the Earth and Planetary Interiors* **95**, 195–209.

Klemme, S. & O'Neill, H. S. C. (2000). The near-solidus transition from garnet lherzolite to spinel lherzolite. *Contributions to Mineralogy and Petrology* **138**, 237–248.

Klemme, S., Blundy, J. D. & Wood, B. J. (2002). Experimental constraints on major and trace element partitioning during partial melting of eclogite. *Geochimica et Cosmochimica Acta* **66**, 3109–3123.

Lenoir, X., Garrido, C. J., Bodinier, J.-L., Dautria, J.-M. & Gervilla, F. (2001). The recrystallization front of the Ronda peridotite: evidence for melting and thermal erosion of subcontinental lithospheric mantle beneath the Alboran Basin. *Journal of Petrology* **42**, 141–158.

Litasov, K. D., Foley, S. F. & Litasov, Y. D. (2000). Magmatic modification and metasomatism of the subcontinental mantle beneath the Vitim volcanic field (East Siberia): evidence from trace element data on pyroxenite and peridotite xenoliths from Miocene picrobasalt. *Lithos* **54**, 83–114.

Makishima, A. & Nakamura, E. (1997). Suppression of matrix effects in ICP-MS high power operation of ICP: application to precise determination of Rb, Sr, Y, Cs, Ba, REE, Pb, Th, and U at ng/g levels in milligram silicate samples. *Geostandards Newsletter* **21**, 307–319.

Menzies, M. A. (ed.) (1990). *Continental Mantle*. Oxford: Clarendon Press.

Nickel, K. G. (1986). Phase equilibria in the system SiO_2–MgO–Al_2O_3–CaO–Cr_2O_3 (SMACCR) and their bearing on spinel/garnet lherzolite relationships. *Neues Jahrbuch für Mineralogie, Abhandlungen* **155**, 259–287.

Nickel, K. G. & Green, D. H. (1985). Empirical geothermobarometry for garnet peridotites and implications for the nature of the lithosphere, kimberlites and diamonds. *Earth and Planetary Science Letters* **73**, 158–170.

Norman, M. D., Pearson, N. J., Sharma, A. & Griffin, W. L. (1996). Quantitative analysis of trace elements in geological materials by laser ablation ICPMS: instrumental operating conditions and calibration values of NIST glasses. *Geostandards Newsletter* **20**, 247–261.

O'Neill, H. S. C. (1981). The transition between spinel lherzolite and garnet lherzolite, and its use as a geobarometer. *Contributions to Mineralogy and Petrology* **77**, 185–194.

Pearson, D. G., Canil, D. & Shirey, S. B. (2003). Mantle samples included in volcanic rocks: xenoliths and diamonds. In: Carlson, R. W. (ed.) *Treatise on Geochemistry. Vol. 2. The Mantle and Core*. Amsterdam: Elsevier, in press.

Petit, C., Koulakov, I. & Deverchère, J. (1998). Velocity structure around the Baikal rift from teleseismic and local earthquake traveltimes and geodynamic implications. *Tectonophysics* **296**, 125–144.

Presnall, D. C., Gudfinnsson, G. H. & Walter, M. J. (2002). Generation of mid-ocean ridge basalts at pressures from 1 to 7 GPa. *Geochimica et Cosmochimica Acta* **66**, 2073–2090.

Press, S., Witt, G., Seck, H. A., Ionov, D. A. & Kovalenko, V. I. (1986). Spinel peridotite xenoliths from the Tariat Depression, Mongolia. I: Major element chemistry and mineralogy of a primitive mantle xenolith suite. *Geochimica et Cosmochimica Acta* **50**, 2587–2599.

Robinson, J. A. C. & Wood, B. J. (1998). The depth of the spinel to garnet transition at the peridotite solidus. *Earth and Planetary Science Letters* **164**, 277–284.

Salters, V. J. M. & Longhi, J. (1999). Trace element partitioning during the initial stages of melting beneath mid-ocean ridges. *Earth and Planetary Science Letters* **166**, 15–30.

Schmidberger, S. S. & Francis, D. (1999). Nature of the mantle roots beneath the North American craton: mantle xenolith evidence from Somerset Island kimberlites. *Lithos* **48**, 195–216.

Schmidberger, S. S. & Francis, D. (2001). Constraints on the trace element composition of the Archean mantle root beneath Somerset Island, Arctic Canada. *Journal of Petrology* **42**, 1095–1117.

Stern, C. R., Saul, S., Skewes, M. A. & Futa, K. (1986). Garnet peridotite xenoliths from the Pali-Aike alkali basalts of southernmost South America. In: Ross, J. (ed.) *Kimberlites and Related Rocks. Geological Society of Australia, Special Publication* **14**, 735–744.

Stern, C. R., Kilian, R., Olker, B., Hauri, E. H. & Kyser, T. K. (1999). Evidence from mantle xenoliths for relatively thin (<100 km) continental lithosphere below the Phanerozoic crust of southernmost South America. *Lithos* **48**, 217–235.

Sun, S. S. & McDonough, W. F. (1989). Chemical and isotopic systematics of oceanic basalts: implications for mantle composition and processes. In: Saunders, A. D. & Norry, M. J. (eds) *Magmatism in the Ocean Basins. Geological Society, London, Special Publications* **42**, 31–345.

Takazawa, E., Frey, F. A., Shimizu, N. & Obata, M. (2000). Whole rock compositional variations in an upper mantle peridotite (Horoman, Hokkaido, Japan): are they consistent with a partial melting process. *Geochimica et Cosmochimica Acta* **64**, 695–716.

Takazawa, E., Okayasu, T. & Satoh, K. (2003). Geochemistry and origin of the basal lherzolites from the northern Oman ophiolite (northern Fizh block). *Geochemistry, Geophysics, Geosystems* **4**, Paper 2001GC000232.

Wallace, M. E. & Green, D. H. (1991). The effect of bulk rock composition on the stability of amphibole in the upper mantle: implications for the solidus positions and mantle metasomatism. *Mineralogy and Petrology* **44**, 1–19.

Webb, S. A. C. & Wood, B. J. (1986). Spinel–pyroxene–garnet relationships and their dependence on Cr/Al ratio. *Contributions to Mineralogy and Petrology* **92**, 471–480.

Zindler, A. & Jagoutz, E. (1986). Mantle cryptology. *Geochimica et Cosmochimica Acta* **52**, 319–333.

Zorin, Y. A. (1981). The Baikal rift: an example of the intrusion of asthenospheric material into the lithosphere as the cause of disruption of lithospheric plates. *Tectonophysics* **73**, 91–104.